INVESTIGATION OF METHODS INVOLVED IN THE DYNAMICS OF GAS-SURFACE ENERGY TRANSFER PROCESSES

By

MICHAEL WILLIAM JEZERCAK

Bachelor of Science

Central State University

Edmond, Oklahoma

1983

Submitted to the Faculty of the
Graduate College of the
Oklahoma State University
in partial fulfillment of
the requirements for
the Degree of
DOCTOR OF PHILOSOPHY
December, 1989

INVESTIGATION OF METHODS INVOLVED IN THE
DYNAMICS OF GAS-SURFACE ENERGY
TRANSFER PROCESSES

Thesis Approved:

Leonel M. Raff
Thesis Advisor

Donald L. Thompson

Paul N. Westhaus

H. L. Suits

Norman N. Durham
Dean of the Graduate College

ACKNOWLEDGEMENTS

Special thanks goes out to Dr. Lionel Raff, who provided me with the bulk of my graduate education, who was understanding of my personal difficulties and who allowed me to work at my own pace which is the greatest contributor to the enjoyment of my profession. Also, thanks goes to Dr. Don Thompson, who unknowingly provided great moral support.

Special thanks also goes out to Vance and Alice, who stuck with me through all the highs and especially through all the lows.

To my parents, William and Irma Jezercak, Mom and Pop, to whom I have the greatest love and appreciation, the merest conception of a work of this magnitude would have been impossible without you. This work is, and has been all along, dedicated to you.

Finally, thanks to Dr. Merle White, whose personal guidance and interest gave me direction in which to guide my abilities. Rest in Peace.

TABLE OF CONTENTS

LIST OF TABLES

LIST OF FIGURES

Figure Page

Figure Page

CHAPTER I

INTRODUCTION

Extensive work involving the examination of gas-surface interaction processes and their mechanisms and rates has been reported. Interest in this area of research is widely distributed throughout the scientific community in the areas of crystal and film growth, subsonic and supersonic flight, and catalysis. More recently, a growing concern has been the investigation of the shuttle glow phenomena which has been associated with many orbital vehicles. Since these processes take place in foreign environments under high orbital velocities, a theoretical approach to the problem can provide much useful information. In this thesis, several gas-surface processes have been investigated and two new methods for the theoretical treatment of these systems have been developed. A brief summary of each of these areas of study is given in this chapter. More detailed accounts of the work are contained in subsequent sections of the thesis.

Wave Packet-Trajectory studies

As systems to be studied become larger, accurate quantum mechanical calculations become increasingly

difficult to carry out. At the same time, classical methods are frequently inadequate in that they fail to accurately reproduce quantum effects when they become important. This situation leads to an interest in semiclassical methods of chemical dynamics. In this approach, part of the problem to be solved is treated by standard classical techniques while the remaining part is given a quantum mechanical treatment. Wave packet studies have been used for atomic and diatomic systems by utilizing the time dependent Schrodinger equation and a wave packet with a spatial or velocity distribution selected to represent translational motion. Other effects, such as vibration and rotation, are included as appropriate wave functions multiplied by the translational part[1-21]. Commonly, the quantum mechanical evolution operator is expanded in a series and truncated after the linear terms. By assuming discrete time steps, this operator produces the wave function at the next (or previous) time step[22-23]. The Schrodinger equation is then solved by numerical methods[24-26]. In this manner, the wave packet is gradually evolved through space and time while under the influence of a potential field. This approach has been used successfully in the study of collinear three-body exchange reactions[1-5]. Extensive work has been done by Heller using Gaussian wave packets in trajectory studies[14-18]. Typically, the wave packet is superimposed on classical trajectories to provide a particle distribution by which quantum effects are introduced. Since the trajectory is classical, effects such as tunneling are not possible.

Wave packet methods have been used with some success in the study of gas-surface scattering. Most work has represented the incoming particle by a selected wave packet distribution while the surface has been treated classically. Most of the time, the surface is represented as a non-moving lattice with a corresponding potential field or as a simple potential-energy function which provides a field through which the wave packet is evolved. Results on surfaces with corrugations and impurities have produced quantitative probability and velocity distributions in a single calculation. Comparison of these calculated results with those obtained by experiment and by exact quantum mechanical calculations have been good to excellent. The rainbow structures seen in experiment, that are so difficult to reproduce in calculations, are easily created[9].

The effects of energy transfer with a moving surface have also been examined. Drolshagen and Heller[8] have evolved a superposition of Gaussian wavepackets at a surface composed of a long chain of 40 atoms. The packet was assumed to come in contact with the first atom only and the others acted as a heat bath to absorb the energy. Interactions between the atoms of the chain were taken to be harmonic and the interaction potential between the incoming wave packet and the first atom in the chain was taken to be a Morse function. The resulting energy distribution showed energy transfer that matched the lattice modes extremely well. Similarly, good results were obtained when the lattice was modified to include dampened motion. Kosloff and

Cerjan[11] modified the surface somewhat to better represent energy transfer by using a generalized Langevin approach. As in the classical studies, this provides a sink to which the energy may be dissipated. The system simulated was that of helium scattering off of a tungsten surface. A first study involved centering the wave packet on the attractive portion of the interaction potential well and observing the gradual desorption. The momentum distributions showed energy transfer to and from the lattice and the rate of desorption was seen to follow a first-order decay. A first-order plot was nearly linear with some minor fluctuations due to the random force terms in the lattice equations of motion. A three-dimensional simulation of the scattering process produced a natural broadening of the wave packet and its velocity distribution that increased as the surface temperature was raised, as would be expected.

Agrawal and Raff[6] developed a wave packet method that was intended to simulate a molecular-beam experiment. The packet was more localized in space and had a velocity distribution that was nearly square. This wave packet was scattered off of a model lattice represented by three moving atoms attached to fixed atoms. The interatomic forces were taken to be harmonic and the interaction potential to be of a simple Lennard-Jones type. The resulting velocity distribution accurately showed energy transfer and surface frequencies. The method was expanded to include three dimensional surface motion by Smith et al.[7]. Surface effects were reproduced including diffraction spectra that

accurately matched calculated rainbow spectra from Bragg diffraction, Debye Waller factors, and variations with surface temperature. Extensions of this work also showed accurate matching of resulting velocity distribution peaks with surface frequencies when the surface force constants were varied.

NO-Ag and NO-Pt Systems

Much of the reported research, experimental and particularly theoretical, has involved scattering of monoatomic particles from various surfaces. The primary reason for this has been limitations in the experimental techniques required to study the properties of polyatomic species, such as distributions of energy within internal degrees of freedom, orientation and alignment of molecules with the surface, etc. With the increased knowledge and availability of laser systems, tremendous increases in sensitivity and resolution provide the means by which more complex systems can be studied. At the same time, theoretical advances have made computational studies of such systems feasible. One of the more widely studied diatomic systems has involved the scattering of nitric oxide from the (111) plane of silver.

Experimental Research

NO-platinum and NO-silver systems are of interest because they involve heterogeneous, diatomic-molecule scattering from two metals that are similar in structure,

both having a fcc lattice type. However, each surface has a slightly different reactivity. Experiments have indicated that platinum has a deeper attractive potential well than that of silver. This allows a variety of studies to be done that involve trapping in the former case and elastic-inelastic scattering in the latter. The nitric oxide molecule is convenient to use. It has an active infrared vibrational mode and the heterogeneous nature of the molecule allows for a preferred binding orientation to the surface. This provides for a much greater range of studies involving approach dependence on resulting energy distributions than would be possible for a simple homogeneous diatomic molecule. There is also a small spin-orbit coupling within the molecule which gives rise to two electronic states separated by approximately 123 cm^{-1} in energy. This allows the study of the redistribution of energy within the different electronic states.

Most of the experimental studies on these systems have separated the scattering processes into four possible scattering events: 1. direct elastic scattering, 2. scattering involving inelastic energy transfer, 3. adsorption onto the surface followed by desorption, 4. adsorption on the surface followed by fragmentation and desorption into nitrogen and oxygen. The fragmentation of NO has been observed to be surface dependent. Lambert and Comrie[27] noted extensive dissociation from recrystallized platinum foil and Gland[28] reported approximately 30% dissociation from Pt(110). More recently, Gland and

Sexton[29] observed approximately 15% dissociation on a Pt(111) surface. This is higher than estimated by Lin and Somorjai[30] who have suggested that NO does not dissociate to any appreciable extent. This higher number of dissociated molecules on the surface agrees with the findings of Gorte and Schmidt[31]. Most of the remaining literature makes no mention of any extensive fragmentation on either platinum or silver and it appears, therefore, that this process plays an insignificant role in NO scattering.

Many research groups have done extensive work on NO scattering from Pt(111)[32-40], and Ag(111)[41-48]. Some of the more extensive work done on the silver surface has been reported by Kleyn et al.[41-44]. Using laser induced fluorescence techniques, they were able to determine the rotational state distribution of the exiting molecules. Measurements were made at temperatures higher than those usually studied. The results revealed a rotational state distribution that was Boltzmann at internal energies less than 0.1 eV, for varying translational kinetic energies. For internal energies greater that 0.1 eV, a large departure from the Boltzmann distribution was found which resulted in a broad maximum whose shape was a function of internal energy. Tenatively, this effect was attributed to a rotational rainbow. This assignment is found to be in good agreement with the calculations discussed below. In the low-energy Boltzmann region, the angular distributions were found to be peaked near the specular angle from which it was concluded that the scattering was predominantly direct.

This result was supported by the correlation of the calculated rotational temperature with the incident energy normal to the surface rather than with surface temperature as would be expected if equilibrium with the surface were allowed to take place. In fact, a good linear relationship was found between incident normal energy and rotational temperature. Kubiak et al.[49] were able to establish a good bilinear fit of the rotational temperature using the incident energy normal to the surface and the surface temperature as variables recognizing that the surface temperature, although not in equilibrium with the rotational temperature, is not a completely independent variable. Three coefficients were generated that represented contributions to the rotational energy from incident energy, surface temperature, and potential-energy well depth. The values obtained for the well-depth coefficient are about 20 to 27 kJ/mole, which is significantly smaller than the 103 kJ/mole estimated by Goddard et al.[46], but is on the order of that obtained for CO on silver by McElhiney et al.[50]. It is generally accepted that the binding strength for NO on silver is less than that of platinum. Values for platinum have been on the order of 105 kJ/mole; therefore, the 103 kJ/mole obtained by Goddard seems a bit high. Muhlhausen, Williams and Tully[51], in a later calculation, attributed this to crystal site defects.

Studies were also done by Luntz et al.[43] to investigate the degree of rotational polarization produced during the scattering process. The intensity measured in

the laboratory was expanded in a Legendre series and truncated after the second Legendre polynomial. A measure of the polarization was then given by polarization anisotropy which is defined to be the ratio of the second Legendre expansion coefficient to the zeroth coefficient. Results showed a fairly strong tendency for the angular momentum vector to become perpendicularly oriented relative to the surface plane when in the high energy, non-Boltzmann regime of the rotational distribution. In the Boltzmann region, very little or no polarization was seen.

Studies of the NO-Pt(111) system provided different results because of the stronger binding energy. Several values for the adsorption energy are obtained using various methods[37-40]. Desorption from the surfaces have been seen to follow first order kinetics. Desorption energies and frequency factors have been calculated and are found to be in good agreement at 105 kJ/mole and 10^{16} s^{-1} respectively. Campbell et al.[37] examined the flux of NO molecules scattering off a platinum surface and have observed an initial sticking coefficient of 0.88 at 300K which decreases to zero as the surface becomes saturated. At time zero, the scattering was seen to have a broad specular lobe which transformed into a distorted cosine distribution as NO accumulated. This was also reported by Segner et al.[35] Campbell et al. also noted an additional desorption mechanism associated with defect sites and calculated a corresponding desorption energy. Guthrie et al.[32] did extensive studies on variances in angular and velocity

distributions with incoming energy and concluded that at lower energies, trapping and desorption are the primary mechanisms involved in scattering from platinum. As the energy of the incoming beam was increased, the inelastic scattering component increased. Accomodation of kinetic energy was seen to be excellent at surface temperatures of 900K and below. Sticking probabilities between 0.7-0.85 at low NO coverages were also found. The values are in good agreement with Campbell et al.[37].

Several researchers have examined internal energy redistribution in scattered NO molecules. As in the case with the silver surface, a Boltzmann distribution was observed. However, the higher energy range observed by Kleyn[41-44] was not examined. The accommodaton of rotational energy was seen to be high at surface temperatures less than 350K. Above that, the rotational temperatures are seen to be less than the surface temperature. Changing the translational energy of the incoming molecules was seen to have very little effect on this result as was expected since the molecules trapped on the surface lose knowledge of their initial states. Examination of preferential alignment of scattered NO molecules did not show the polarization that was observed in scattering from a silver surface[38]. An examination of the vibrational state distributions has also been reported for this system[33]. The angular distribution of molecules excited to the first vibrational state was seen to have an almost perfect cosine distribution with no preference

towards the specular angle. This implies that all vibrationally excited molecules originate from desorption. They conclude that inelastically scattered molecules are not on the surface long enough for vibrational excitation to take place. A plot of the internal rotational energy distributions obtained from the experimental results shows the proper shape, but the curve deviates slightly from the calculated Boltzmann distribution. It was concluded that desorption rates of the ground vibrational state and the first excited state follow a first-order rate law, but have different preexponential factors. Adjustment of those factors accurately reproduces the data.

Theoretical studies

Many researchers have examined the systems described above on a theoretical basis in order to understand more fully the mechanisms involved. One of the simplest approaches is the hard-cube model used to describe scattering in monoatomic systems[51-54]. These models are not expected to give accurate quantitative results, but rather to provide insight into the trends associated with parameters such as energy, beam flux, etc. Hurst, Kubiak et al.[55] have reported hard-cube model calculations in an attempt to reproduce their experimental results. In this model, the incoming molecule is represented by a hard ellipsoid which was assumed to be initially rotationless. The surface is represented as a hard cube which is allowed to move, thus opening the possibility for energy transfer to the surface.

The potential is represented by a repulsive and an attractive region. The repulsive part was the hard-cube surface while the attractive part was represented by an energy well that accelerates the incoming molecule. Among the results, it was observed that rainbow patterns appear as singularities for incoming NO molecules with no initial rotation and possible singularities for NO having a non-zero rotational temperature, although the peaks are broad. Also, there is total alignment of the angular momentum vector parallel to the surface. The result is independent of surface temperature. To simulate the experimental conditions, the system was averaged over initial states of the molecule and of the surface. The results were found to reproduce the rotational dependence on initial energy and surface temperature, however, the parameters used to obtain this fit resulted in very high trapping probabilities.

Kleyn, Luntz, and Auerbach[41-44], in an attempt to reproduce their experimental rotational polarization data, carried out a classical trajectory calculation[56] using an uncorrugated Morse-type potential. As in their experimental work, the results were expressed in terms of the polarizational anisotropy as a function of rotational energy. A structureless surface, along with simple potentials, prevented them from quantitatively reproducing their data, however, the spectra were similar. For low J values, the molecules were unpolarized, and as energies were increased, the polarization increased towards the perpendicular. The calculations showed almost complete polarization at inter-

mediate energies, and a sudden sharp decrease as higher J states were reached, which was qualitatively but not quantitatively correct. Barker et al.[57], have reported a classical and a quantum mechanical close-coupling study in an attempt to reproduce the observed rainbow distributions. A potential surface was constructed based on observations that surface corrugation plays a minor role in energy transfer; that surface phonons are probably not involved in the scattering process since they observed a weak dependence of final energy states on surface temperature; and that, as a first approximation, only the distance of the center of mass of the molecule from the surface is important. The classical results showed a similar shape to the experimental data, but the calculated high-energy rainbow was much sharper. The close coupling results gave a better shape, but failed to reproduce the linear dependence at low energy. The conclusion was that classical mechanics fails to give an adequate description of rainbow scattering for systems that otherwise may seem classical.

The potentials used in this calculation and in the previous study were also used in a recent quantum close-coupling calculation in an attempt to reproduce the observed polarization[58]. Even though more effort was involved in this calculation, the results were not much better. Two conclusions were reached: first, the rotational polarization observed is due to a weakly corrugated interaction potential between NO and silver, thus, only weak transitions in the magnetic quantum number are possible even

though dramatic changes in the J state are observed. Secondly, for dynamical effects, the initial orientation distribution can become very important. A molecule initially rotating in a plane perpendicular to the surface will exhibit maximum inelastic energy transfer as opposed to a plane parallel to the surface. This could be verified experimentally only by using polarized incident beams. The first conclusion seems to justify the assumptions made by Barker et al.[57], but the second conclusion is contradictory to their final assumption of no azimuthal dependence.

Zamir and Levine[59] were able to calculate the contribution of various modes of energy transfer by using a maximum entropy formalism. They expressed the entropy in the form of probability distributions and maximized it using Lagrange multipliers subject to constraints. The constraints are constructed as sums of the various modes of energy dispersal among the different scattering channels, multiplied by weighting factors built from accommodation coefficients. All experimental data are said to be well described for NO scattering from metal surfaces. Of particular interest was the ability of the method to reproduce the non-Boltzmann distributions in rotational states at high internal energies observed by Kleyn, et al.[41] in their molecular beam experiments of NO scattering from silver.

The effects of surface motion were introduced in a study by Polanyi and Wolf[60] in which the silver surface was represented initially as a non-moving rigid surface,

secondly, as a simple harmonic oscillator and third, by generalized Langevin techniques[111-112]. The potential was the same in all cases and included exponential repulsion with an inverse cubic attraction term along with terms to include diatomic orientational dependence, well depth, force constant adjustment, and other fine tuning factors. The system modeled was NO on Ag(111) and the well depth was on the order of 56 kJ/mole. The non-moving surface model exhibited trapping only when the molecule struck the surface in such a manner as to convert translational motion to rotational motion. This type of behavior broadened the observed rainbow pattern. The harmonic oscillator model surface, although allowing energy transfer, had no channel to dissipate the energy away from the impinging atom, thus the energy eventually found its way back into the molecule and allowed it to desorb. The Langevin model allowed dissipation of the translational energy into surface phonon modes and ultimately into the bulk. This manifested itself in the form of lower probabilities in the higher J states. This model was also able to qualitatively reproduce the Boltzmann plot observed by Kleyn, Luntz, and Auerbach[56], and it was concluded that the linear portion of the plot was indeed due to trapping and subsequent desorption while the nonlinear portion was due to direct scattering.

Muhlhausen, Williams and Tully[51] have recently presented a potential-energy surface that has been able to produce more quantitative results for NO on both the silver and platinum surfaces. Their interest was a first attempt

at developing a potential that could reproduce all of the available experimental information rather than selected results. The potential consisted of a direct NO-surface interaction term that included a factor to insure that maximum binding occurs with the nitrogen end pointing towards the surface as suggested by Ibach and Lehwald[39], a diatomic Morse potential, and terms that describe weak van der Waals type interaction. The only parameter that was varied between the two surfaces was the potential well depth which was 105 kJ/mole for platinum(111) and 72 kJ/mole for silver (111). The value chosen for silver was an estimate based on the well depth for CO on Ag(111), a value estimated by Kleyn et al.[42] and estimates by Kubiak et al.[49]. The calculations were carried out by integrating classical equations of of motion in three dimensions for NO and four moving surface atoms. The remainder of the lattice was represented by a stochastic trajectory approach with terms chosen to reproduce the phonon spectrum of the metal surface. Vibrations of the surface atoms were taken to be harmonic and vibrations of the NO molecule were ignored due to the high vibrational frequency.

Angular and velocity distributions produced by this surface were in good agreement with experiment including mean velocities and widths, indicating that translational energy exchange was accurately reproduced. Calculations were also in good agreement with estimated sticking probabilities and predicted dependencies of sticking on initial translational energy, rotational energy and

orientation. Qualitative agreement with experiment was achieved in reproducing the Boltzmann plot of probability vs. rotational energy. A linear plot was produced at lower rotational energies along with a nonlinear portion at higher energies. Analysis showed that the nonlinear region could indeed be attributed to rotational rainbow effects. The rainbow produced was broadened in accordance with experiment and in contrast to the sharper spectra usually obtained by calculation[57]. Although the trends were well predicted for rotational polarization via the rotational anisotropy, the results were in poor quantitative agreement. A calculated Arrhenius plot of the desorption rate reproduced the binding energy and also predicted a prefactor that was in excellent agreement with experiment. An examination of the energy of the scattering molecules showed rotational and translational cooling. As the surface temperature was lowered, perfect accommodation was seen to occur and these results were in quantitative agreement with measurements on these systems. Overall, results were at least in qualitative agreement with experiment showing that the chosen potential gives a reasonably good description of the system. This potential will be used for this study.

Shuttle glow phenomena

Early in the space program involving the space shuttle, it was found that the tail sections of shuttle orbiter were emitting a visible glow. This type of phenomena was not surprising, as it had been noted in satellites for some

time. The concern in the case of orbiting satellites was not enough to warrent an extensive investigation. However, interference with extremely sensitive equipment aboard the shuttle orbiter has led to much study of the processes involved.

The glow has been observed to occur in the ram direction of the orbiting shuttle,[88,89] increasing with orbiter angle of attack, and is seen to extend approximately 20 centimeters into space. Spectral analysis shows a continuous spectrum increasing in intensity out to 800 nm. Primary constituents in the shuttle environment are N, O, NO, N_2, and O_2. The spectral bands observed seem to show indications of all of the molecular species. A likely contributor to the glow spectrum is the NO molecule which has a continuous spectrum falling off in the red region. Although this molecule may not contribute in the red region, it may certainly play a part in the blue and green ends of the spectrum[90,91]. The lifetimes have been speculated to be at 50 microseconds if surface scattering is elastic. [92] Dependence on atomic oxygen concentration has been observed at altitudes above 160 km. [93] On shuttle mission STS-41D, surface samples were observed to produce glow emissions of different intensities. Among these samples were aluminum, carbon cloth, and Z302 (a polyurethane black paint) overcoated with silicon. The polyethylene was seen to produce the lowest intensity while the silicon surface was seen to produce the brightest glow.

There have been many speculations concerning the source

of the shuttle glow phenomenon[94-99], the most likely being that of recombination of oxygen and nitrogen atoms into excited molecular states. It is the intent of this study to concentrate on the oxygen mechanisms. The work will investigate 1) if oxygen can be introduced to a silicon surface at orbital velocities (7.5 km/sec) and be observed to trap onto the surface, 2) if diatomic oxygen can be adsorbed onto the silicon surface and what processes occur, and 3) if an oxygen atom can collide with an oxygen atom on the surface, combine with it and exit the surface.

CHAPTER II

FORMULATION

Three separate studies of various types of gas-surface processes have been carried out in this thesis work. In this chapter, the mathematical models for these investigations are described.

Semiclassical wave packet trajectory calculations

In this section, the formulation of the scattering of a quantum mechanical wave packet from a classical surface is described.

The classical atomic surface is composed of nine moving and 28 nonmoving atoms whose geometry is chosen to represent the (100) plane of a body-centered cubic lattice. The spatial arrangement of the atoms is shown in Figure 1. The open circles represent the nine moving atoms. The closed circles denote nonmoving atoms, the larger of which are atoms in the same plane as the moving atoms while the smaller circles represent atoms below the surface plane. The moving atoms are assigned a mass M corresponding to the mass of neon and the nonmoving atoms have infinite mass. The lattice potential is a pairwise sum of 60, nearest-neighbor

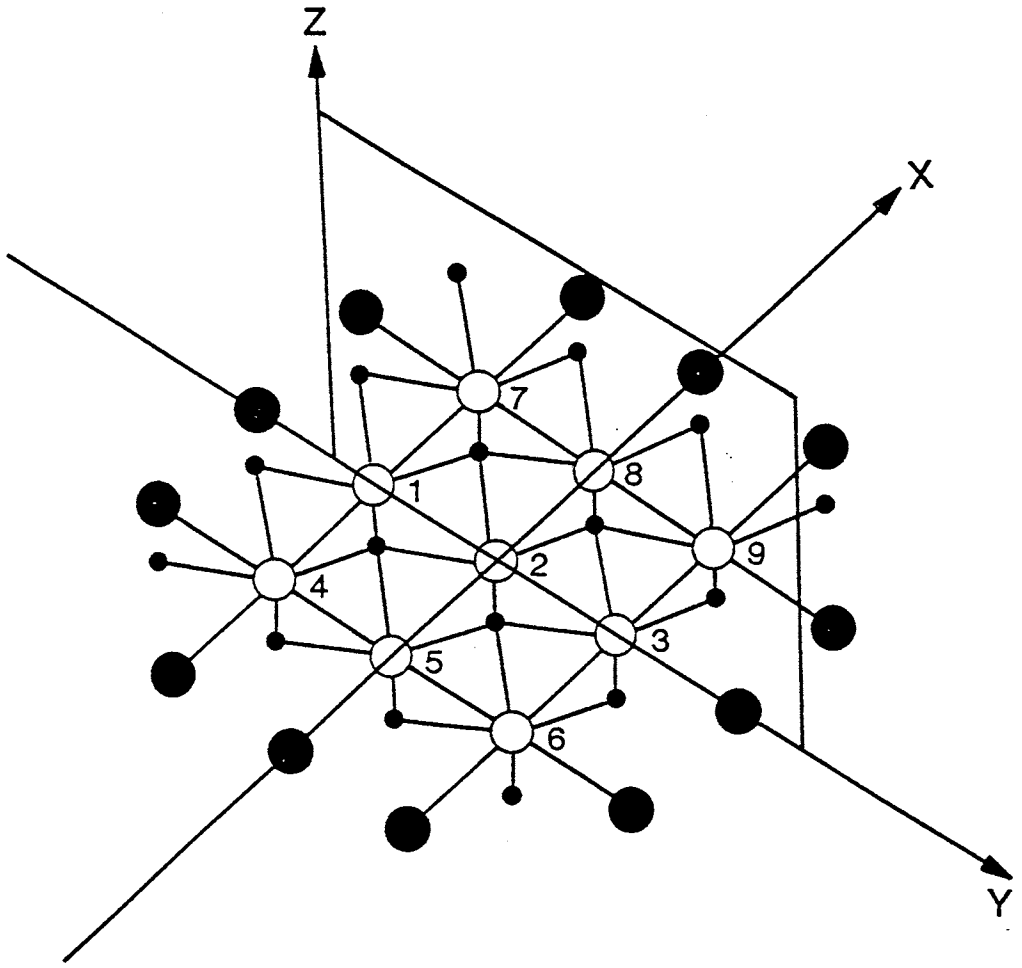

Figure 1. Model Atomic Arrangement for Neon Lattice

harmonic interactions. The atoms are initially placed in their equilibrium positions and then each are given an energy of 3kT, where k is the Boltzmann constant and T is the surface temperature in degrees Kelvin. By the equipartition theorem, it is assumed that the energy of 3kT is equally partitioned into the three degrees of freedom of each moving atom. Therefore, a momentum of $\pm\sqrt{[2mkT]}$ is assigned to each coordinate direction with the sign being chosen randomly. The total energy of the surface prior to collision with the incoming atom, which is given by the classical Hamiltonian, is 27kT.

The total lattice Hamiltonian is

$$(1) \qquad H = (P_{xi}^2 + P_{yi}^2 + P_{zi}^2)/2M_i + V_L \quad ,$$

where

$$(2) \qquad V_L = \sum_{i=1}^{60} V_i$$

and

$$(3) \qquad V_i = (f_k/2)(R_i - Re)^2$$

f_k is the vibrational force constant.

Once the initial positions and momenta of all the atoms are determined, the motion of the atoms over time is then determined using Hamilton's equations:

$$(4) \qquad \partial H/\partial P_{xi} = P_{xi}/M = \dot{X}_i$$

$$(5) \qquad \partial H/\partial P_{yi} = P_{yi}/M = \dot{Y}_i$$

$$(6) \qquad \partial H/\partial P_{zi} = P_{zi}/M = \dot{Z}_i$$

$$(7) \qquad \partial V/\partial X_i = -\dot{P}_{xi}$$

$$(8) \qquad \partial V/\partial Y_i = -\dot{P}_{yi}$$

$$(9) \qquad \partial V/\partial Z_i = -\dot{P}_{zi}$$

for i = (1,2,.....9) .

The coordinates and momenta of the atoms at later times are determined by solving the coupled differential equations (4-9) using a fourth-order Runge-Kutta method with minimum error bounds[108]. These equations were solved over 1250 time steps where 1 time step = 4.0×10^{-16} sec. The positions and momenta of the surface atoms were stored at all times. Accuracy of integration was checked by energy conservation and back integration.

The incident particle is described by a two-dimensional quantum mechanical wave packet that represents an ensemble of momenta reflecting that of an atomic beam experiment. The wave packet is assumed to move in the y-z plane (Figure 1) and is incident in the region of the center atom in the moving surface. The functional form of the wave packet is given by

$$(10) \qquad \Psi = A(z)*B(y) \quad ,$$

where

$$(11) \qquad A(z) = \exp(-iw_o z)\sin\{\Delta w(z - z^o)\}/(z - z^o)(\Pi\, \Delta w)$$

and

$$(12) \qquad B(y) = \begin{cases} (2a)^{-1/2} & \text{for } (-a \leq y \leq a) \\ 0 & \text{for } y > a \text{ or } y < -a \end{cases}$$

with

$$a = (Re / 2.0 + \Delta y)\cos\theta_i \quad .$$

Re is the equilibrium lattice spacing and w is the wavenumber. w_o is the initial wavenumber corresponding to the center of the momentum distribution of the initial wavepacket and θ_i is the incident angle of the wavepacket relative to the surface normal.

The momentum distribution for the incident wave is given by the Fourier transform of A(z), F(w),

$$(13) \qquad F(w) = \begin{cases} \exp(iwz_i^o)/(2\,\Delta w) & \text{for } (w_o - w) \leq w \leq (w_o + w) \\ 0 & \text{for } w > (w_o + \Delta w) \text{ or } w < (w_o - \Delta w) \end{cases}$$

where z_i^o specifies the initial location of the wave packet. It is seen that the wave packet given by Eq. (10) has a square distribution of velocities. The configuration-space

view of this wave packet is shown in Figure 2 and the momentum space distribution obtained from Eq (13) is shown in Figure 3. The distribution is nearly square and has a width Δw. The small features at 5.5 and 8.8 A^{-1} are due to small amounts of traverse motion. By a simple change in variables, the corresponding energy distribution can be obtained.

The evolution if the wave packet is carried out using the integration method outlined by Harmuth(24) and expanded by Askar and Cakmak(22). The wave packet is evolved over a 12 x 26 angstrom grid with grid spacing 0.2 angstroms. The time step was 4.0×10^{-16} sec to provide correct back integration and energy conservation. The interaction of the wave packet with the moving surface was taken to be a pairwise sum of Lennard-Jones 6-12 potentials with the nine moving atoms:

$$(14) \qquad V = \sum_{i=1}^{9} V_i \quad ,$$

where

$$(15) \qquad V_i = 4 \epsilon \{(\sigma/R_i)^{12} - (\sigma/R_i)^{6}\} \quad .$$

The coordinate R_i is the distance between point (Y,Z) and the instantaneous position of the ith lattice site. Direct substitution of the positions of the moving lattice

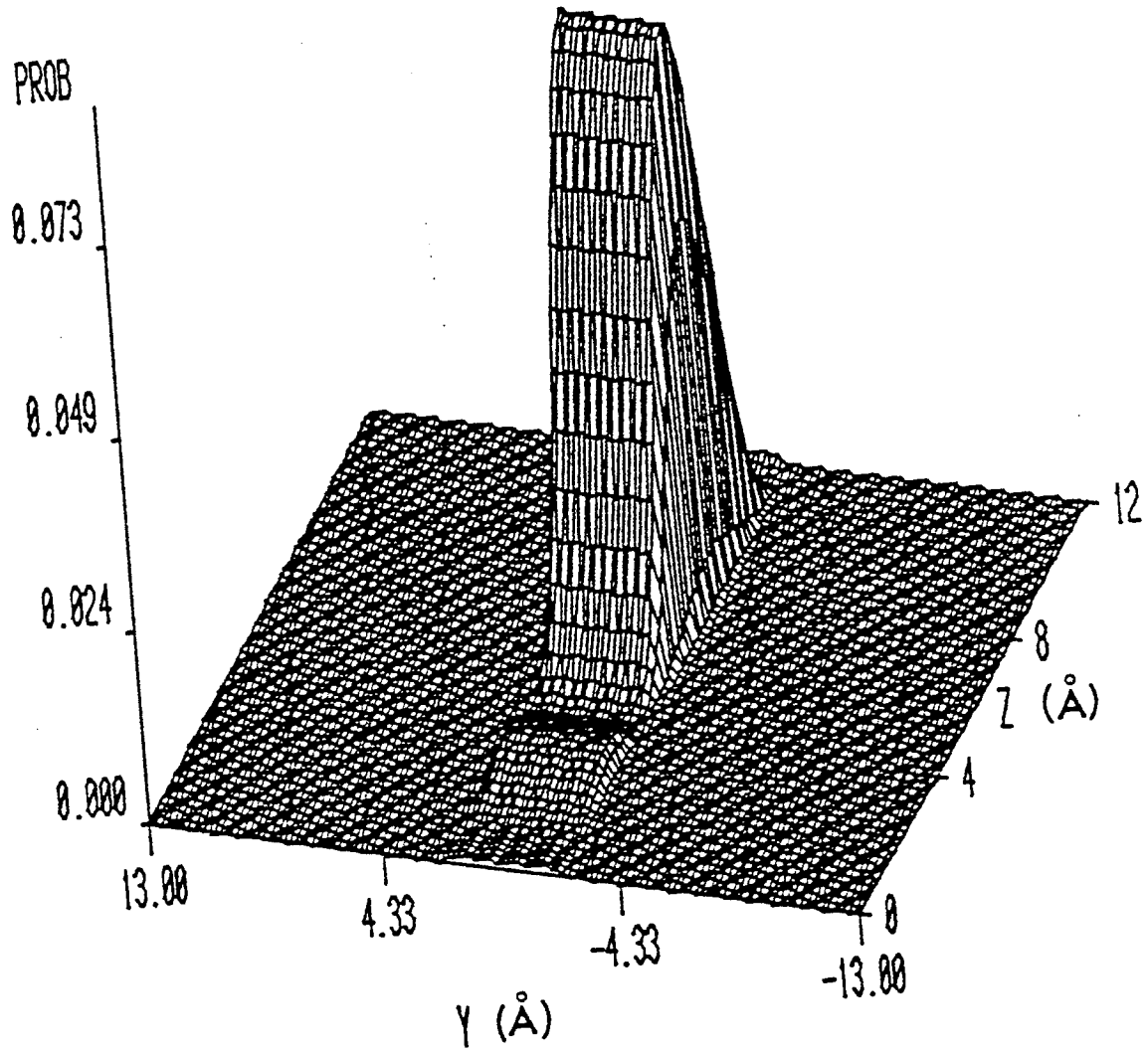

Figure 2. Configuration-Space View of Initial-State Wave Packet

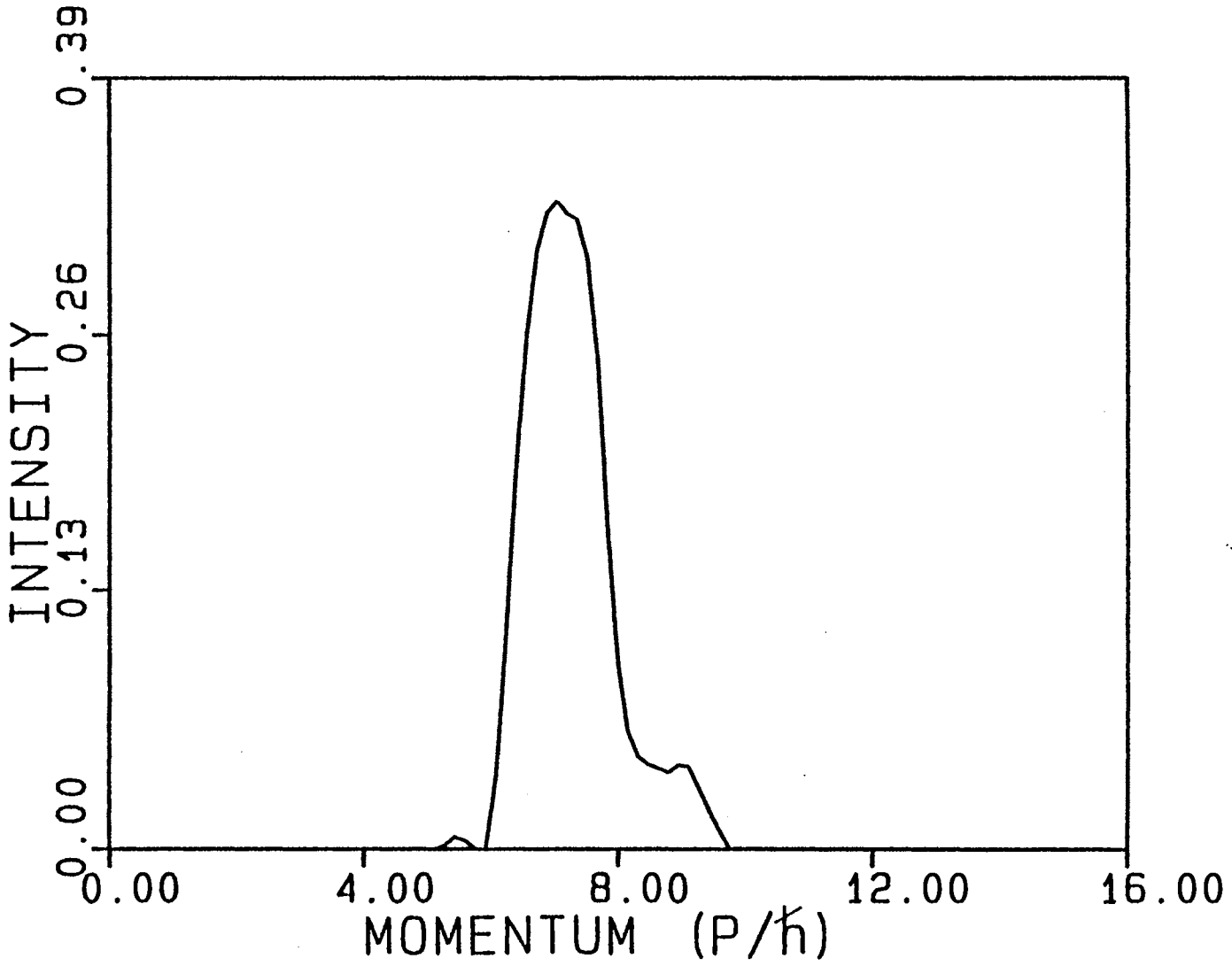

Figure 3. Momentum-Space Representation of Initial-State Wave Packet

atoms obtained by the solution of Eqs. (4-9) into the interaction potential yields a time varying potential field through which the wave packet is evolved. The values for all the constants are given in Table I.

All information about the final state of the atomic beam may be obtained from the final-state wave function. The average kinetic energy of the wave-packet at any time is given by

$$(16) \quad \langle E \rangle = (-\hbar^2/2m) \langle \Psi(y,z,t) | \partial^2/\partial y^2 + \partial^2/\partial z^2 | \Psi(y,z,t) \rangle \ .$$

The numerical calculation of the required second derivatives is carried out using a second difference method.

$$(17) \quad \partial^2 \Psi(y,z,t)/\partial y^2 = (\Psi_{j+1,k} + \Psi_{j-1,k} - 2\Psi_{j,k})/\Delta y^2 \ ,$$

where $\Psi_{j,k}$ denotes the wave-packet at grid point (i,k).

The momentum distribution at any time can be obtained from the two-dimensional Fourier transform of $\Psi(y,z,t)$,

$$(18) \quad P(w)\, dw = \int_0^{2\pi} |F(w, \theta_w)|^2 w \, dw \, d\theta_w \ ,$$

where $F(w, \theta_w)$ is the Fourier transform of $\Psi(y,z,t)$,

and $w = (w_y^2 + w_z^2)^{1/2}$,

TABLE I

POTENTIAL, LATTICE AND MASS PARAMETERS FOR
FOR WAVE-PACKET TRAJECTORY STUDIES [7]

PARAMETER	VALUE
Lattice interatomic distance	3.517 Å
Lattice force constant	5.36 eV/Å^2
Lennard-Jones parameters;	
ϵ_o /k	38.5 K
σ	2.74 Å
Mass of lattice atom	20.18 amu
Mass of incoming "atom"	1.008 amu

and $\theta_w = \tan^{-1}(w_y/w_z)$.

Inserting $E = \hbar^2 w^2/2m$ into (18), the momentum distribution can be transformed into an energy distribution.

Perturbation-trajectory Method for the study of Inelastic Scattering of NO from Ag(111)

In this section, a method that permits a significant reduction in computer time requirements for the study of large gas-surface systems is described. Implimentation of this method involves dividing the gas-surface system up into different 'zones'. The labeling of the zones follows that used by Langevin and other methods.[113-115] The interaction region involving the dynamics of the system that of are interest is labelled the P-zone. A larger region that is involved with energy transfer into and out of the P-zone is labelled the Q-zone. Also, occasionally, a third B-zone is defined, which is not involved in energy transfer, but serves to provide a boundary to the system in order to reduce edge effects. In the perturbation method, the positions and momenta of all the Q-zone atoms are calculated from a lattice trajectory in the absence of the perturbation and the results stored at all times. The substitution of these unperturbed coordinates into the potential provides a dynamic field through which gas or surface atoms, making up the P-zone, can be allowed to move.

For the NO-Ag(111) gas-surface system, the surface is assigned to be the Q-zone and the incoming molecule will be labelled the P-zone. This system was chosen for study because it is a well studied system, it is large enough to satisfy the requirements of the perturbation method and yet involves relatively simple dynamics with no chemical reactions, and a reasonably good potential-energy surface has been developed and examined by Muhlhausen, Williams, and Tully[51]. In that study, the surface was treated using a ghost atom-Langevin approach. Consequently, this choice will allow a convenient comparison of exact, Langevin, and perturbation methods to be made.

The Hamiltonian for the system may be written as

$$(19) \quad H = T_M(\dot{Q}) + T_L(\dot{q}) + V_M(Q) + V_L(q) + VI(Q,q)$$

where T_M and T_L are the kinetic energy terms for the NO molecule and lattice atoms, respectively. V_M is the reaction potential between the nitrogen and the oxygen. V_L is the potential between the surface atoms, taken in this problem to be harmonic potentials. VI is the interaction potential between the NO molecule and the surface atoms. Q and q are respectively, the set of cartesian coordinates of the gas molecule and lattice atoms and $\dot{Q}$ and $\dot{q}$ are the corresponding velocities. The lattice Hamiltonian, H_L, is defined to be

$$(20) \quad H_L = T_L(\dot{q}) + V_L(q) \quad .$$

Initially, the motion of the surface is determined in the absence of the incoming gas molecule by the solution of Hamilton's equations using H_L as defined in Eq (20). The initial lattice conditions for the reference trajectory are obtained by the method described below. The solution yields the positions and momenta of all the surface atoms at all times. Substitution of these results directly into Eq(19) yields a P-zone Hamiltonian, H_p , that has the form

$$(21)\quad H_p = T_M(\dot{Q}) + V_M(Q) + VI(Q,q(t))$$

where the q(t) are obtained directly from the reference trajectory for the unperturbed lattice. Equation (21) is a two-body Hamiltonian involving only the coordinates and momenta of NO. The effect of the lattice enters via the VI(Q,q(t)) term.

In general, the accuracy of the perturbation method is expected to be very good for conditions under which the motion of the Q-zone is minimally affected by the atoms of the P-zone. This criteria is satisfied when the incident gas atom to surface atom mass ratio is very low as is the case when nitrogen and oxygen of masses 14 and 16 amu's, respectively, are scattered from silver of mass 108 amu's. Accuracy should also improve when the incident gas atom-surface atom interaction is decreased or when the incident translational energy of the gas atom is decreased.

The silver surface used is the first three layers from the (111) plane of a face-centered cubic lattice. It is

shown in Figure 4. The first layer consists of 30 atoms, 16 of which are fixed in their equilibrium positions while the remaining 14 are allowed to move. The second layer consists of 14 nonmoving atoms and nine which are moving. The third layer is constructed of 15 atoms fixed in their equilibrium positions. All of the moving atoms are attached by pairwise harmonic springs to nearest neighbors. The harmonic force constant is adjusted until the Fourier transform of the lattice motion yields the surface Debye frequency utilized by Muhlhausen et al.[51] Each atom is initially placed in its equilibrium position and assigned a momentum corresponding to an energy of kT in each coordinate direction, the direction of motion being assigned randomly. The positions and momenta are then calculated at later time steps using Hamilton's equations. The surface is 'scrambled' for 200 time steps initially, then the positions of each of the atoms are stored at each time step in an array to provide the q(t) required in Eq (21). To facilitate calculations and to permit comparison to the study carried out by Muhlhausen et al., the NO molecule is assumed to be a rigid rotor. The virtual forces used to accomplish this are introduced by the methods described by Sathyamurthy and Raff[109]. Molecular collisions with the Ag(111) surface are averaged over impact point and surface vibrational phase using standard methods[121].

The interaction potential between the NO and the surface atoms follows that of Muhlhausen et al. It has the form

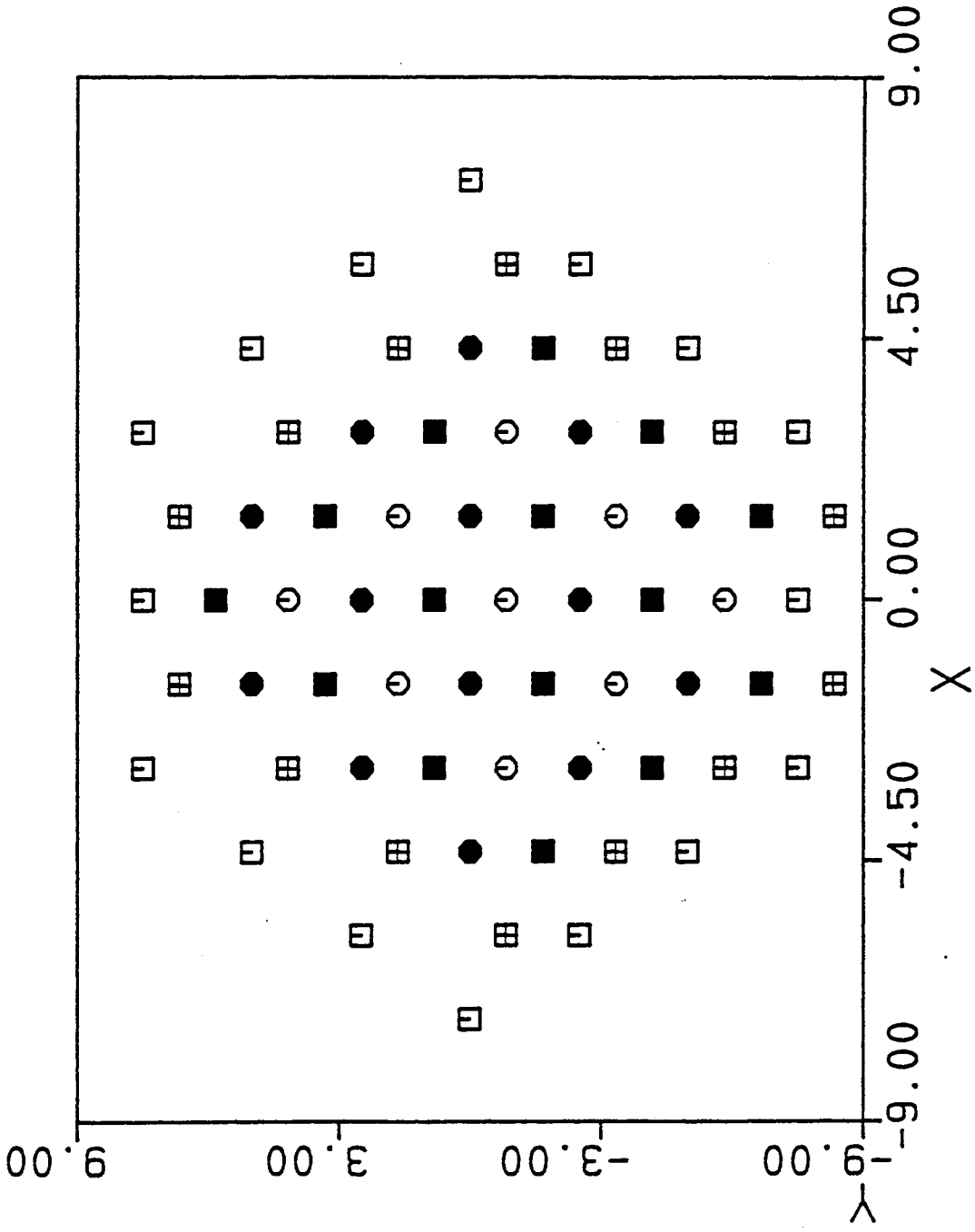

Figure 4. Top View of Ag(111) Lattice Arrangement

$$(22) \qquad VI(Q,q) = \sum_i V_i(\vec{r}_N,\vec{r}_O,\vec{r}_i) + C(z-z_o)^{-9} - (D + E\cos^2\theta)(z-z_o)^{-3} \quad ,$$

where

$$(23) \qquad V_i(\vec{r}_N,\vec{r}_O,\vec{r}_i) = A\exp(-\alpha|\vec{r}_i - \vec{r}_O|) + B\{\exp[-2\beta(|\vec{r}_i-\vec{r}_N| - r_e] - 2\cos^2\eta \exp[-\beta(|\vec{r}_i-\vec{r}_N| - r_e)]\} \quad .$$

with the sum extending over the 14 moving surface atoms. θ is the angle of the diatomic axis with respect to the surface normal with $\theta = 0$ corresponding to the nitrogen end pointing toward the surface. The cosine term in Eq. (23) is present to insure that maximum binding occurs when the nitrogen is pointing towards the surface. η is the angle between the vectors $r_N - r_i$ and $r_N - r_O$.

The first term in (23) is a repulsion term between the oxygen and the surface. The second term is an attractive-repulsive potential between the nitrogen and the surface. The second and third terms in (22) describe weak Van der Waals type interactions. The values for all the constants are identical to those employed by Muhlhausen et al. and are given in Table II.

TABLE II

INTERACTION POTENTIAL PARAMETERS FOR AG(111)-NO AND POTENTIAL SURFACE FEATURES [61]

Parameter	Value
A	634.28 eV
B	0.663 eV
C	0.954 eV
D	8.732 eV
E	1.104 eV
z_o	1.000 Å
α	3.366 Å
β	1.683 Å
r_e	1.500 Å
On-top site binding energy	0.746 eV
N - Ag distance	1.94 Å
NO - Ag stretching frequency	205 cm^{-1}
N-O-Ag bending frequency	294 cm^{-1}

Scattering of oxygen from a Si(111)-(7x7) reconstructed surface.

The Binnig et al.[115] model of the Si(111)-(7x7) surface is utilized to study the scattering of oxygen atoms and molecular oxygen. The surface model consists of the top three layers of the silicon surface. The relaxed surface calculated and utilized by Agrawal et al.[116] in the study of SiH_2 reaction dynamics and silicon-atom surface diffusion was used in this study. The first layer consists of 12 atoms containing dangling bonds created when the Si(111) is allowed to reconstruct to the (7x7) configuration. The second layer consists of 81 atoms, 26 of which have dangling bonds. The third layer consists of 99 atoms all fixed into position (Figure 5). The surface potential used is Keating's potential[110]. Its functional form is given by

$$(24)\quad VS = \sum_{ij} \frac{f_a(r_{ij}^2 - R_{ij}^2)}{2R_{ij}^2} + \sum_{ijk} \frac{f_b(r_{ij}r_{ik} - R_{ij}R_{ik})}{8(R_{ij}R_{ik})}$$

where the first sum runs over the nearest-neighbor two-body interactions and the second sum includes three-body potential terms between nearest and next-nearest neighbors. f_a and f_b are bond stretching and bond bending force constants, respectively. R_{ij} is the equilibrium vector between lattice atoms i and j and r_{ij} is the instantaneous vector between these atoms.

The interaction between the incoming oxygen molecule

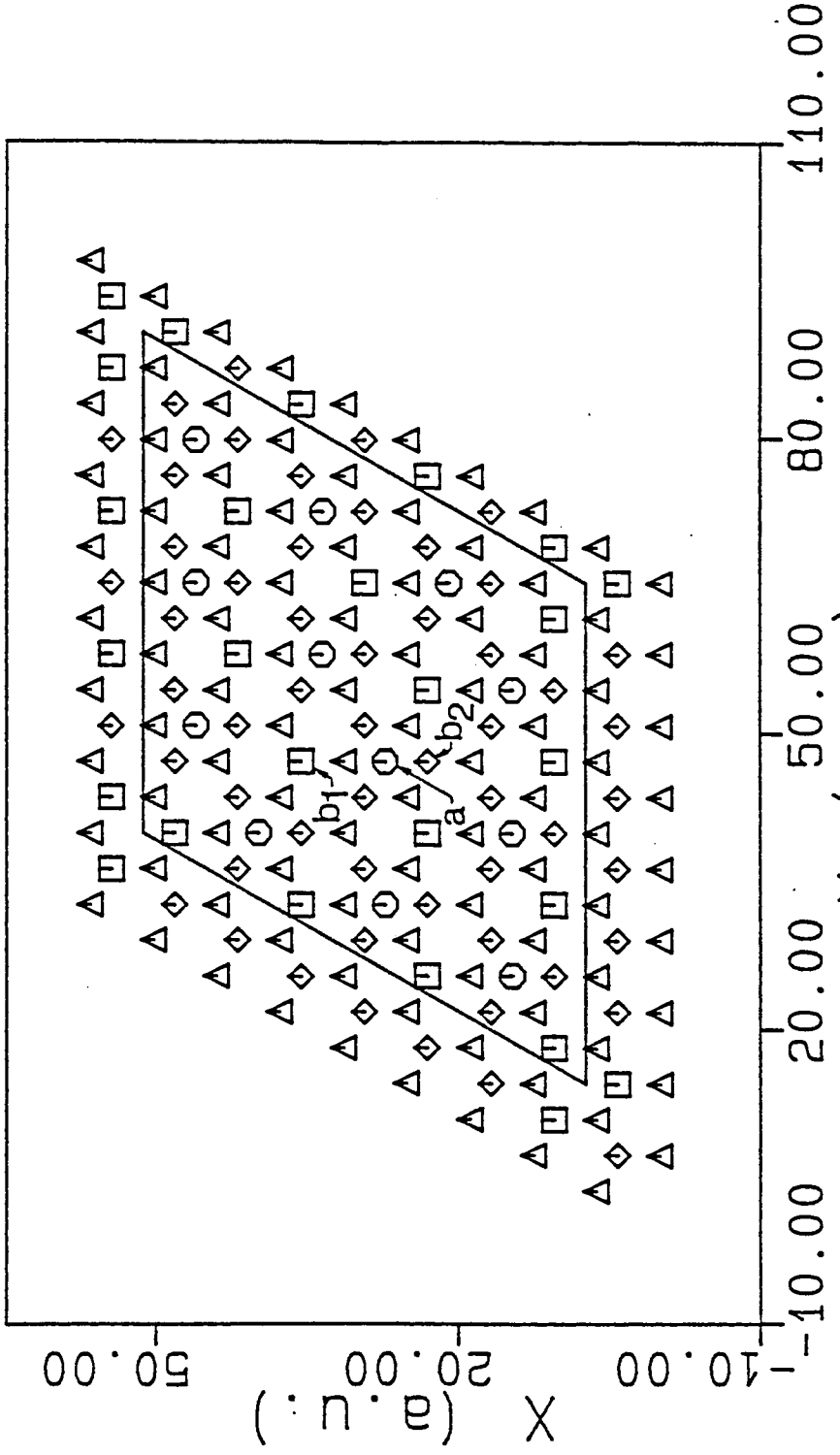

Figure 5. Top View of Si(111) Lattice Arrangement

and the surface is assumed to have the form

$$(25) \qquad V = \sum_{i=1}^{38} (VM1 + VM2 + VB1 + VB2)$$

$$+ \sum_{i=39}^{192} (VR1_i + VR2_i) + VDI + VSI$$

where

$$(26) \qquad VM1_i = [De(1 - \exp(-\alpha(R1_i - Req1))) - De] \times \tanh(p(R2_i - Req2)) \times (1 + a\cos\xi + b\cos^2\xi)/(1 + a + b)$$

$$(27) \qquad VM2_i = [De(1 - \exp(-\alpha(R2_i - Req2))) - De] \times \tanh(p(R1_i - Req1)) \times (1 + a\cos\xi + b\cos^2\xi)/(1 + a + b)$$

$$(28) \qquad VB1 = bk/2 \times (1 - \tanh(p(R2_i - Req2)) \times (1 - \tanh(p2(R - RD2)) \times (\Omega - \Omega_{eq})^2$$

$$(29) \qquad VB2 = bk/2 \times (1 - \tanh(p(R1_i - Req1)) \times (1 - \tanh(p(R - RD1)) \times (\Omega - \Omega_{eq})^2$$

$$(30) \quad VR1 = A \times \exp-(\beta \times R1_i)$$

$$(31) \quad VR2 = A \times \exp-(\beta \times R2_i)$$

$$(32) \quad VDI = (DD \times (1 - \exp(DM1(R - RD1))) - DD) \times \tanh(D \times ZM)$$

$$(33) \quad VSI = (DS \times (1 - \exp(DM2(R - RD2))) - DS) \times (1 - \tanh(D \times ZM))$$

Eq. (26) is an attractive-repulsive potential operating between the first oxygen atom and all silicon atoms with dangling bonds. Eq. (27) is the corresponding potential for the second oxygen atom. R1 and R2 are the distances from the first and second oxygen atoms, respectively, to the silicon atom on the surface. Req1 and Req2 are the equilibrium bond lengths for the Si-O bond. Both of these potentials are attenuated by a switching function which prevents both oxygen atoms from bonding to the same surface site. Both potentials also contain a bending term to insure that the equilibrium surface bonding position lies directly above the dangling bond with ξ being the angle that the oxygen $r_{Si} - r_O$ vector makes with a vector normal to the surface. Potentials VB1 and VB2 are bending potentials for the oxygen molecule on the silicon surface where Ω is the Si-O-O bond angle and Ω_{eq} is the equilibrium angle. Their

presence insures the proper bonding angles. Both of these terms are attenuated by a functions that diminish the bending terms as the molecule dissociates or leaves the surface completely. VR1 and VR2 are exponential repulsive terms between the oxygen atoms and nonbonding surface atoms. VDI is a diatomic Morse potential representing the oxygen-oxygen double bond and VSI is a Morse potential representing the oxygen-oxygen single-bond configuration. R represents the distance between the two atoms. RD1 is the equlibrium bond length for the double bonded molecule and RD2 is the equlibrium bond length for the oxygen-oxygen single bond. The single bond equilibrium length was estimated from values obtained from organic ethers.[119] Both are modified by attenuation functions to insure that the oxygen molecule changes to single bond character as it approaches the surface. This potential-energy surface also allows the formation of a peroxide bridge between adjacent dangling bond sites. It is assumed that the bond strength between the oxygen atoms is relatively unchanged by the peroxide formation.

Values for all the adjustable parameters for this potential energy surface are given in Table III. The Morse potential parameter De in VM1 and VM2 was adjusted to produce a silicon-oxygen well depth of 4.74 eV.[117-119]. The stretching force constant, ks, obtained from Bhandia and Schwartz[117] was assumed to be harmonic and was then be related to the Morse parameter α through the equation $\alpha = \sqrt{ks/2De}$. The parameters a and b in the bending term were

TABLE III

INTERACTION POTENTIAL PARAMETERS FOR Si-O AND POTENTIAL SURFACE FEATURES

PARAMETER	VALUE
De	4.742 eV
α	0.676 a.u.$^{-1}$
p	1.5 a.u.$^{-1}$
Req1	3.0425 a.u.
Req1	3.0425 a.u.
a	0.25
b	0.5
b_k	8.0952 eV/rad^2
A	1454.31 eV
β	1.6202 a.u.$^{-1}$
DD	5.0908 eV
DS	1.4738 eV
RD1	2.2816 a.u.
RD2	2.7968 a.u.
DM1	0.7022 a.u.$^{-1}$
DM2	0.7034 a.u.$^{-1}$
D	2.0 a.u.$^{-1}$
f_a	0.6358 eV/a.u.^{2}
f_b	0.4824 eV/a.u.^{2}

where 1 a.u. = 0.5292 A

adjusted such that a Si-Si-O bending frequency of 483 cm^{-1} was obtained when the oxygen was in its equilibrium position above the silicon[117]. The attenuation parameter was carefully chosen such that when an oxygen molecule was placed in its equilibrium bonding position above a silicon surface site, the attenuation function would have a value of unity allowing for a complete bond between the silicon and the first oxygen atom. The function would then approach a value of zero for the second oxygen atom within the oxygen-oxygen bond length. In this manner, the oxygen molecule can be allowed to bond to a surface site without dissociating. Potential terms VB1 and VB2 were included to take into account the repulsive force that replaces the attractive force for the second oxygen atom as the first oxygen atoms bonds to the surface. The first attenuation functions are identical to those utilized in VM1 and VM2. These functions attenuate a harmonic bending term that insures an equilibrium Si-O-O bonding angle of 124 degrees. The second attenuation function serves to reduce the effect of the bending term as the oxygens dissociate. The bending force constant, bk, was taken from Bhandia and Schwartz [117]. VR1 and VR2 are repulsive terms that act between the oxygen atoms and the non-bonding silicon atoms. The parameters A and β were chosen to produce repulsive forces equivalent to those calculated using Gaussian 82 Hartree-Fock calculations for He-He repulsive interactions using a 3-21G basis set. VDI and VSI are the diatomic potential energy terms. Both are modified by attenuation

functions that convert the oxygen molecule from a double to a single bond as the molecule approaches the surface. The Morse term parameters were selected to match the diatomic bond strength and frequency[120]. ZM is the distance of the oxygen molecule center-of-mass from the surface plane. The parameter D was chosen to provide a reasonable transition region for the conversion of the oxygen-oxygen double bond to the oxygen-oxygen single bond as the molecule approaches the surface[116]. The potential values used to adjust the parameters are given in Table III.

CHAPTER III

RESULTS AND DISCUSSION

Wave-Packet Trajectory Calculations

In the wave-packet trajectory studies carried out by Smith et al.[7] a wave-packet representing an ensemble of hydrogen atoms was scattered from a surface at 1000 K. It was found that inelasticity of collision increased as the surface temperature was increased. Diffractive scattering was observed at all surface temperatures and the structure of the final-state wave packet diffraction peaks was found to be in excellent accord with the calculated diffraction patterns from the known surface gratings using an identical distribution of wavelengths.

In the above studies, the surface energy was partitioned among all of the 27 possible surface vibrational modes. In the present study, we have investigated the effects of each individual surface phonon mode upon energy transfer. We have also examined the variation in energy transfer with the surface Debye temperature and lattice frequency. Finally, trapping and desorption are studied by varying the potential-energy well depth. It is found that the desorption rate decreases in a near exponential manner with increased well depth.

Figure 2 shows a perspective view of the initial-state wave packet given by Eq. (10). The Fourier transform of this wave packet is given by Eq. (13) and is shown in Figure 3. The final-state momentum distribution for a wave packet with incident energy 0.089 eV scattering from a 1500 K surface with energy partitioned into all 27 surface phonon modes is shown in Figure 6 (Smith et al[7]). The incident incoming angle is parallel to the surface normal. Comparison of the final and initial-state momentum distributions shown in Figure 3 shows that substantial energy transfer, both to and from the surface, has taken place. Parameters for this and all subsequent calculations, unless otherwise noted, are given in Table I.

The model lattice consists of nine moveable atoms initially placed in their equilibrium positions as shown in Figure 1. Since each atom is attached to fixed sites and to nearest neighbors by harmonic interaction potentials, each can be considered to have three degrees of vibrational freedom. We therefore have 27 possible vibrational modes. The form of the normal vibrations for this system are shown in Figure 7. Each picture in Figure 7 represents movement in any one of the three possible Cartesian directions with + and - indicating motion either up or down, left or right, and in or out, with 0 indicating no motion in any direction.

Initially, a lattice energy of 27kT is supplied to one of the vibrational modes. The wave packet is then allowed to scatter from the surface and the final-state momentum distribution is calculated. An examination of intermodal

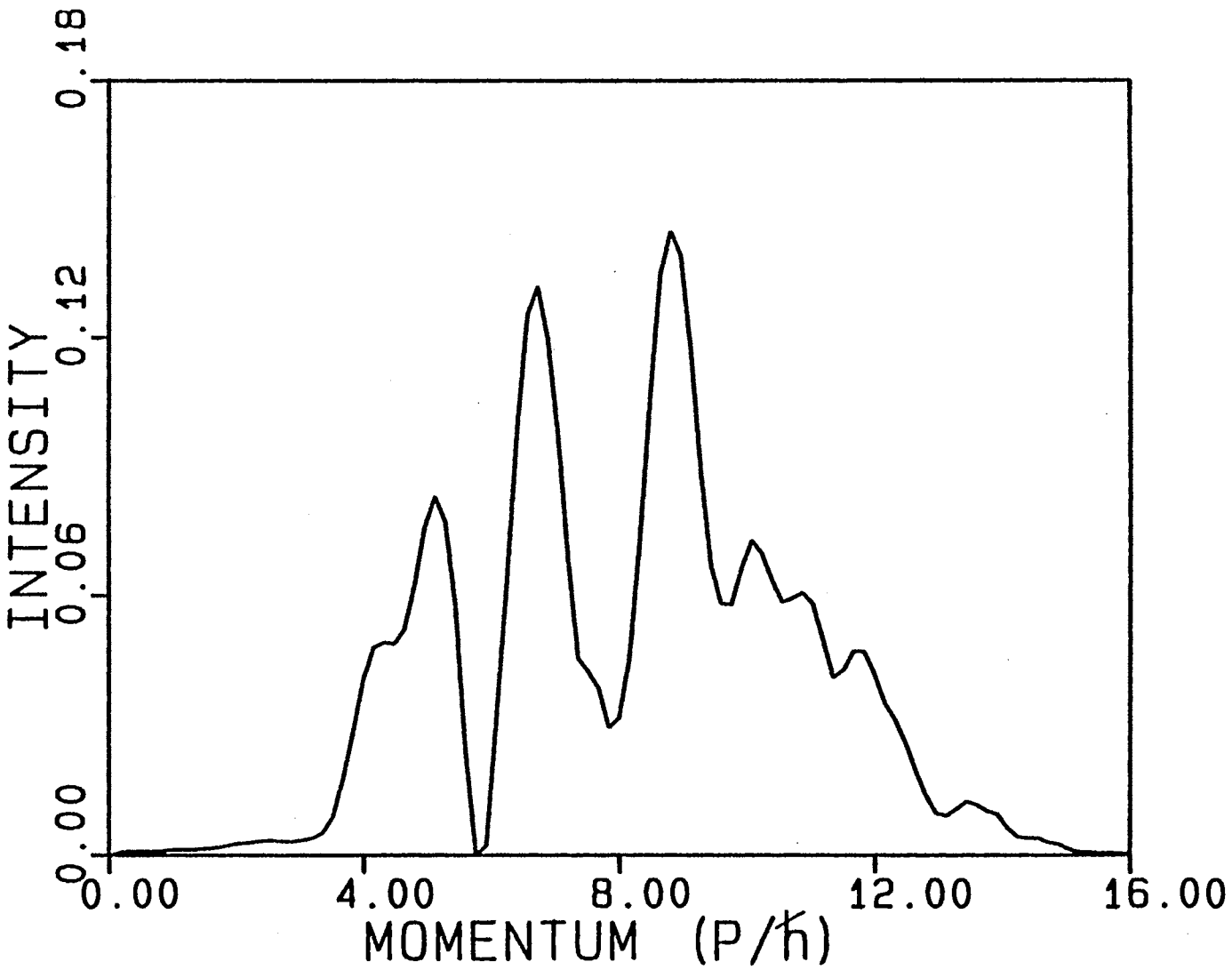

Figure 6. Final-State Momentum Distribution of Scattered Wave Packet

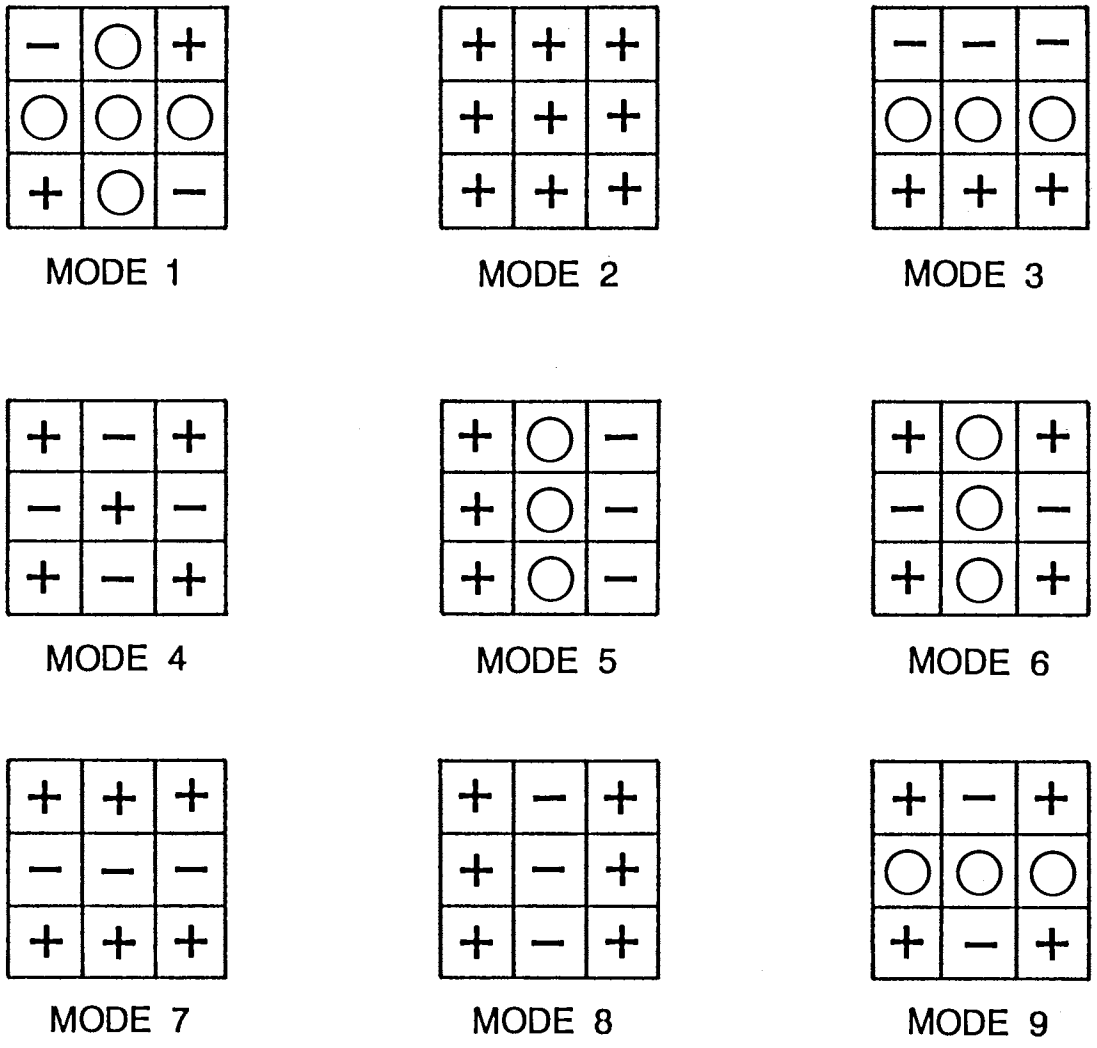

Figure 7. Standing Wave Vibrational Modes of Model Surface for Wave Packet Calculations

energy transfer was carried out, using methods described by Raff[122], to find out if energy remains within each mode over the period of wave packet interaction. The velocities of each of the atoms in the moving surface are written as a linear combination of normal mode velocities.

$$(34) \quad \dot{q}_j = N_{ij} \dot{Q}_{ij}$$

where the $\dot{Q}_{ij}$ are the normal-mode velocities and $\dot{q}_j$ are the atom velocities. N_{ij} is 1 or -1 denoting the direction of the atoms in the normal mode. Equation (34) may be inverted to give the normal-mode velocities, $\dot{Q}_{ij}$ in terms of the $\dot{q}_j$. Since the $q_j(t)$ are known as a function of time, the inverse of Eq. (34) yields the normal-mode velocities at the corresponding times. The envelope functions of the time variations of the normal-mode velocities give the intermode energy transfer rates. It was assumed that the in-plane modes did not couple with out-of-plane modes and modes of different symmetry are not coupled using the lattice potentials given by Eq. (3). For modes of similar symmetry, the envelope functions show that in the time that is required for the wave packet to interact with the surface, energy transfer out of a particular mode is insignificant, being about 0.4 % for energy placed in mode 7 and less that 0.01 % for energy placed in mode 2. Therefore, on the time scales utilized in this calculation, intermodal energy

transfer can be considered to be negligible and the modes uncoupled.

For any one mode or combination of modes, the lattice is given a total energy of (i x j)kT, where i is the number of degrees of freedon associated with each atom and j is the number of moving atoms. When the lattice energy is partitioned into any of the 18 normal phonon modes corresponding to motion parallel to the surface plane, little or no energy transfer is produced. The final-state momentum distribution for a wave packet with normal incidence impinging on a surface with all atoms moving in the Y direction corresponding to mode 2 is given in Figure 8. Comparison to the initial-state wave packet momentum distribution given in Figure 3 shows the two results to be nearly identical. Consequently, it can be concluded that very little or no energy transfer to or from the lattice has taken place. Similar results are obtained for all 18 in-plane lattice modes for a wave packet with normal incidence.

For vibrational modes perpendicular to the lattice plane, very similar results are obtained for modes 1, 3, 5, 6, and 9. All show little or no energy transfer. Modes 2, 4, 7, and 8 show very different results. When the lattice energy is initally partitioned into one these modes, the collsional energy transfer is very similar to that seen when all modes are participating. The final-state momentum distribution for a wave packet normal to the surface plane striking a surface vibrating in mode 2 is shown in Figure 9. Comparison to the final-state wave packet result in Figure

6 shows that mode 2 contributes significantly to energy transfer. Very similar results are obtained for modes 4, 7, and 8. These results suggest that phonon modes that have momentum components at the impact point parallel to the incident momentum vector of the impinging wave packet will contribute significantly to energy transfer.

Further investigation was carried out by allowing the wave packet to approach the surface at incident angles of 30 and 45 degrees from the surface normal in the Y-Z plane. Figures 10 and 11 show the final-state momentum distributions obtained for incidence angles of 30 and 45 degrees, respectively, when the lattice energy is partitioned into mode 2 with motion in the X direction. Since the surface motion is perpendicular to the incident wave-packet momentum vector, very little energy transfer occurs and the final-state momentum distribution looks very similar to that for the initial-state. When the lattice motion is in the Y direction, there is a momentum component in the Y-Z plane and we expect the collisions to become more inelastic. This is indeed found to be the case. Figures 12 and 13 show the final-state momentum distributions for wave-packets incident on a surface vibrating in mode 2 with the lattice motion being in the Y direction. Figures 12 and 13 show results for incidence angles of 30 and 45 degrees, respectively. Both figures show significant inelasticity with the amount of energy transfer increasing as the incident angle is increased from 30 to 45 degrees. This is expected behavior since the component of the lattice momentum in the direction

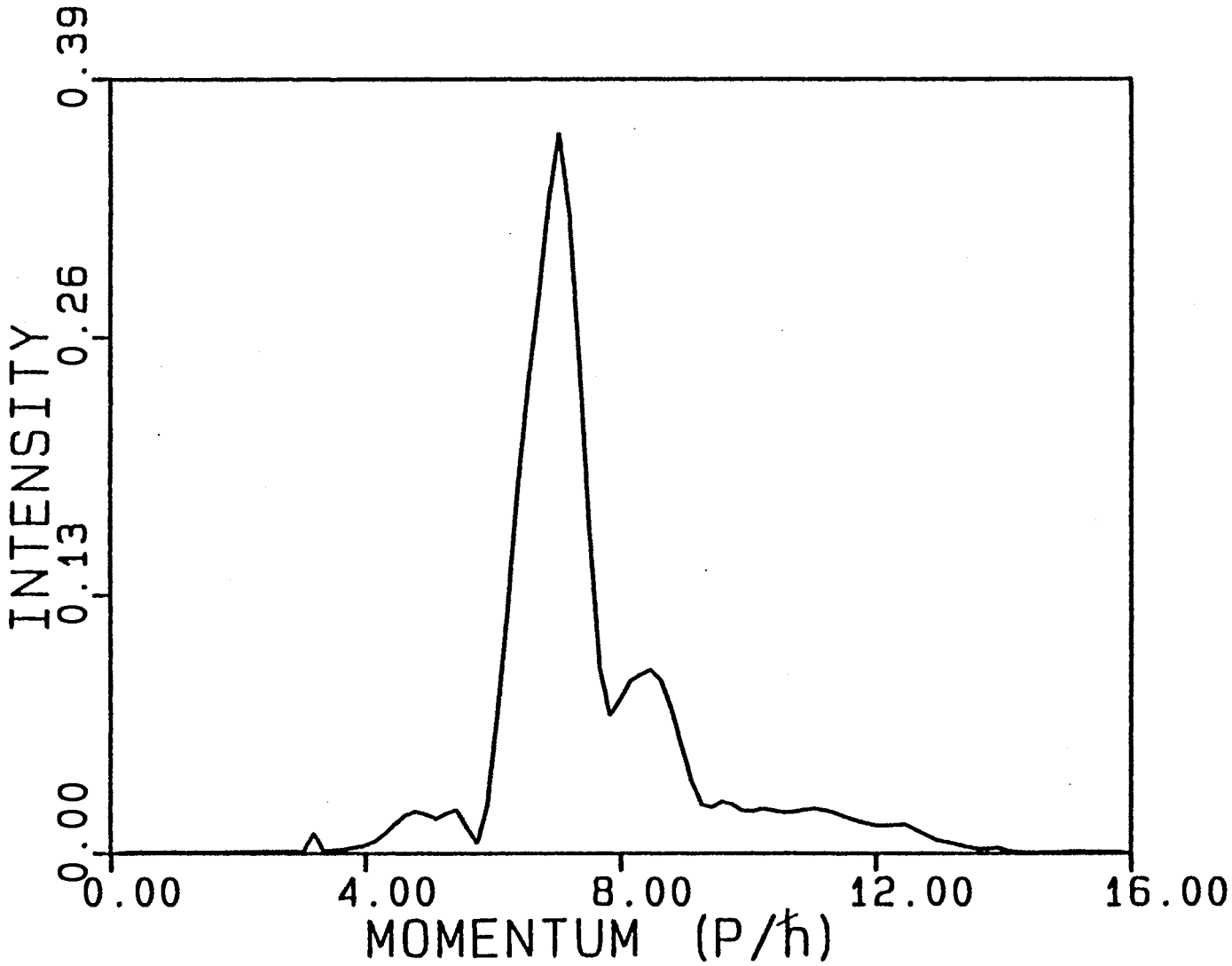

Figure 8. Final-State Momentum Distribution for Wave Packet of Normal Incidence with Lattice Motion in Mode 2 with Motion Parallel to the Surface Plane

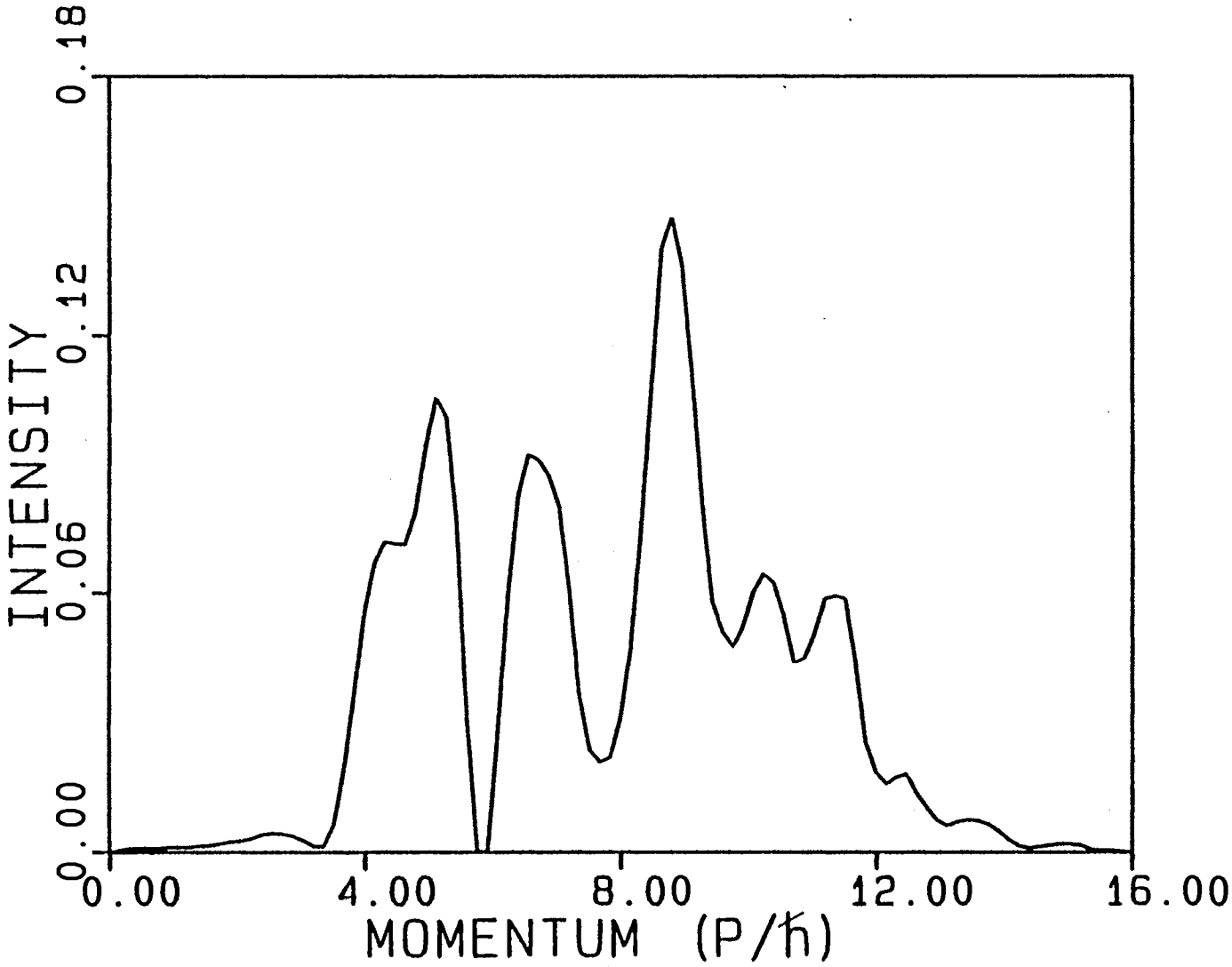

Figure 9. Final-State Momentum Distribution for Wave Packet of Normal Incidence with Lattice Motion in Mode 2 with Motion Perpendicular to the Incident Wave Vector

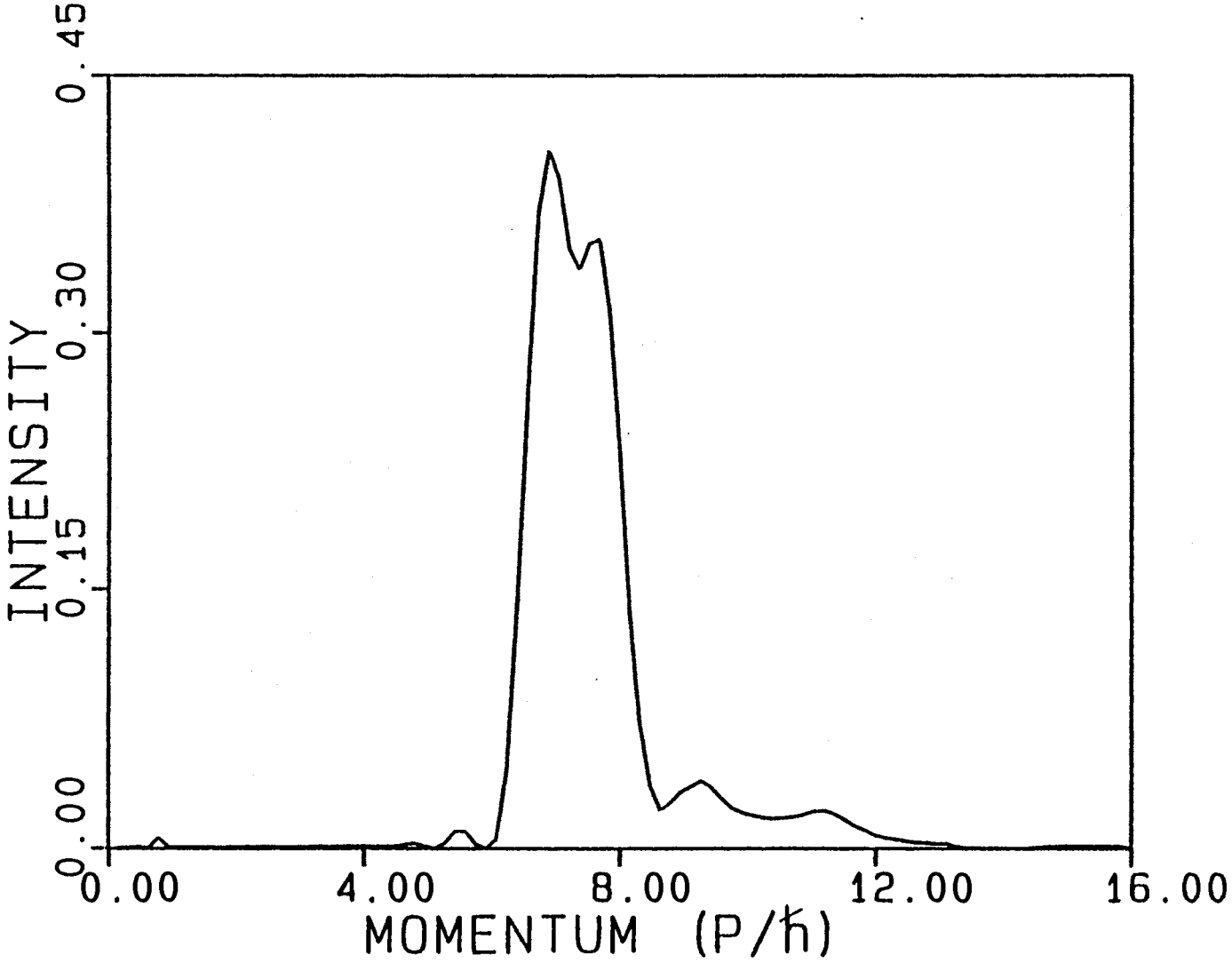

Figure 10. Final-State Momentum Distribution for Wave Packet at 30 Degree Incidence with Surface Motion in Mode 2 Perpendicular to the Incident Wave Vector

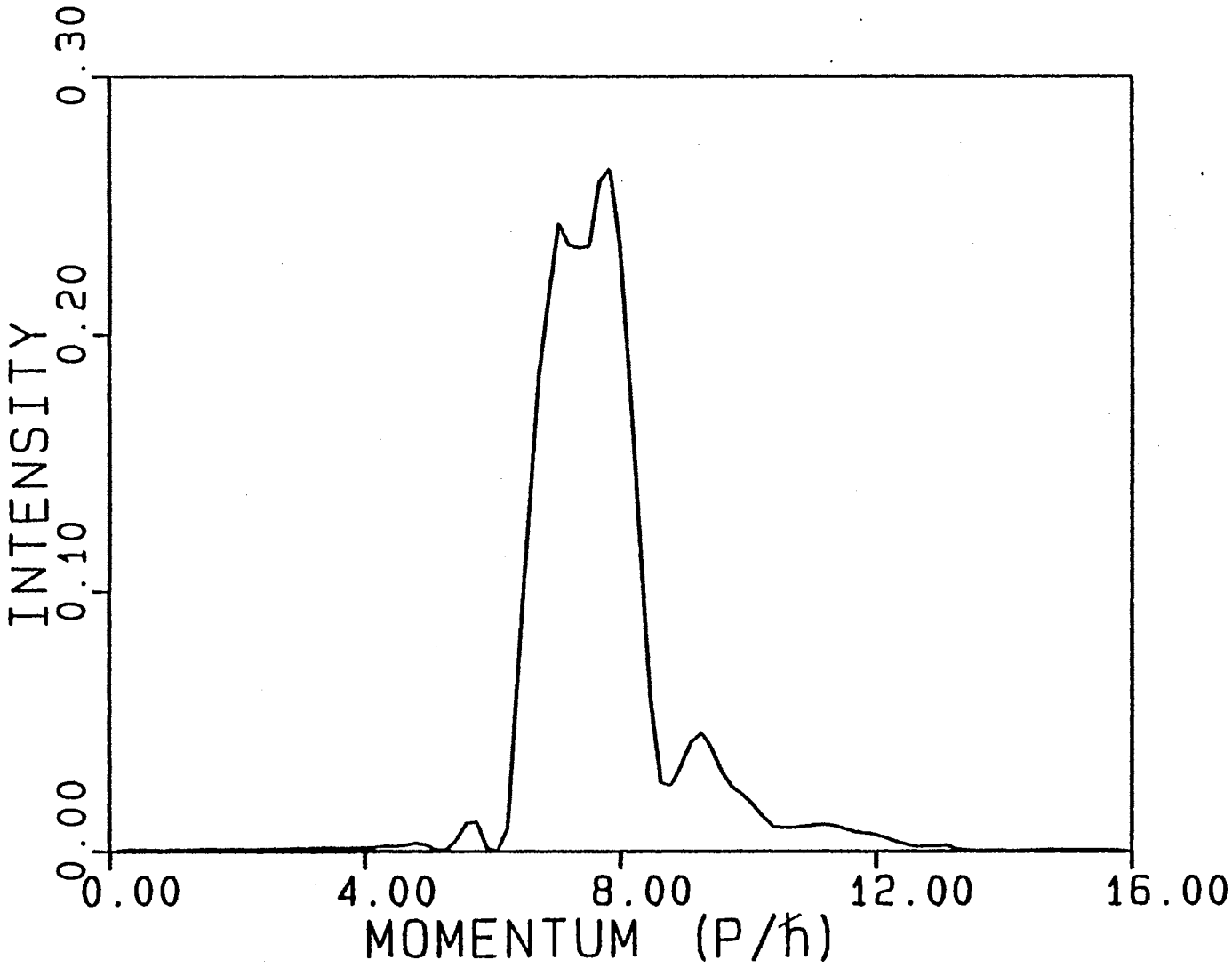

Figure 11. Final-State Momentum Distribution for Wave Packet at 45 Degree Incidence with Surface Motion in Mode 2 Perpendicular to the Incident Wave Vector

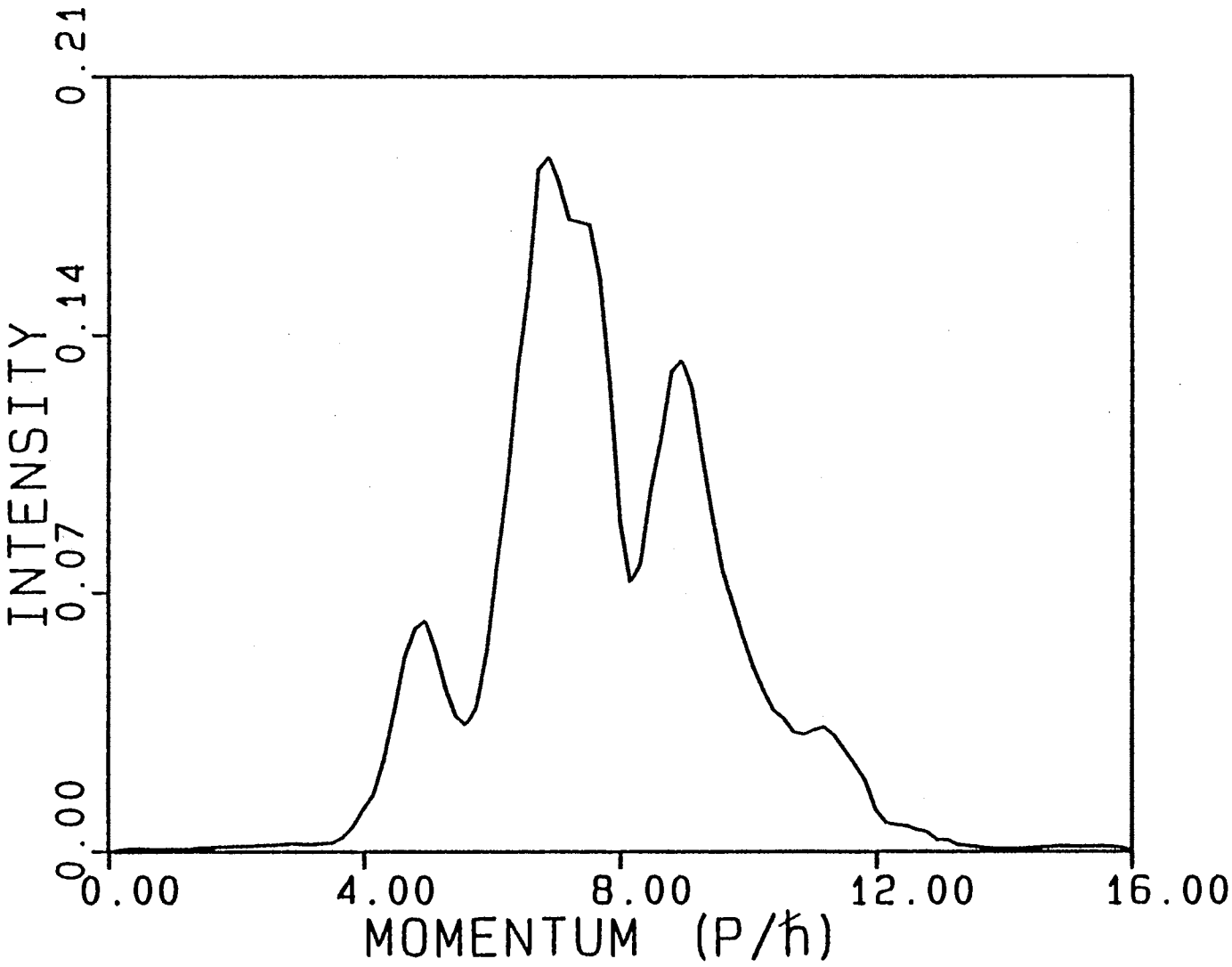

Figure 12. Final-State Momentum Distribution for Wave Packet at 30 Degree Incidence with Surface Motion in Mode 2 Parallel to the Incident Wave Vector

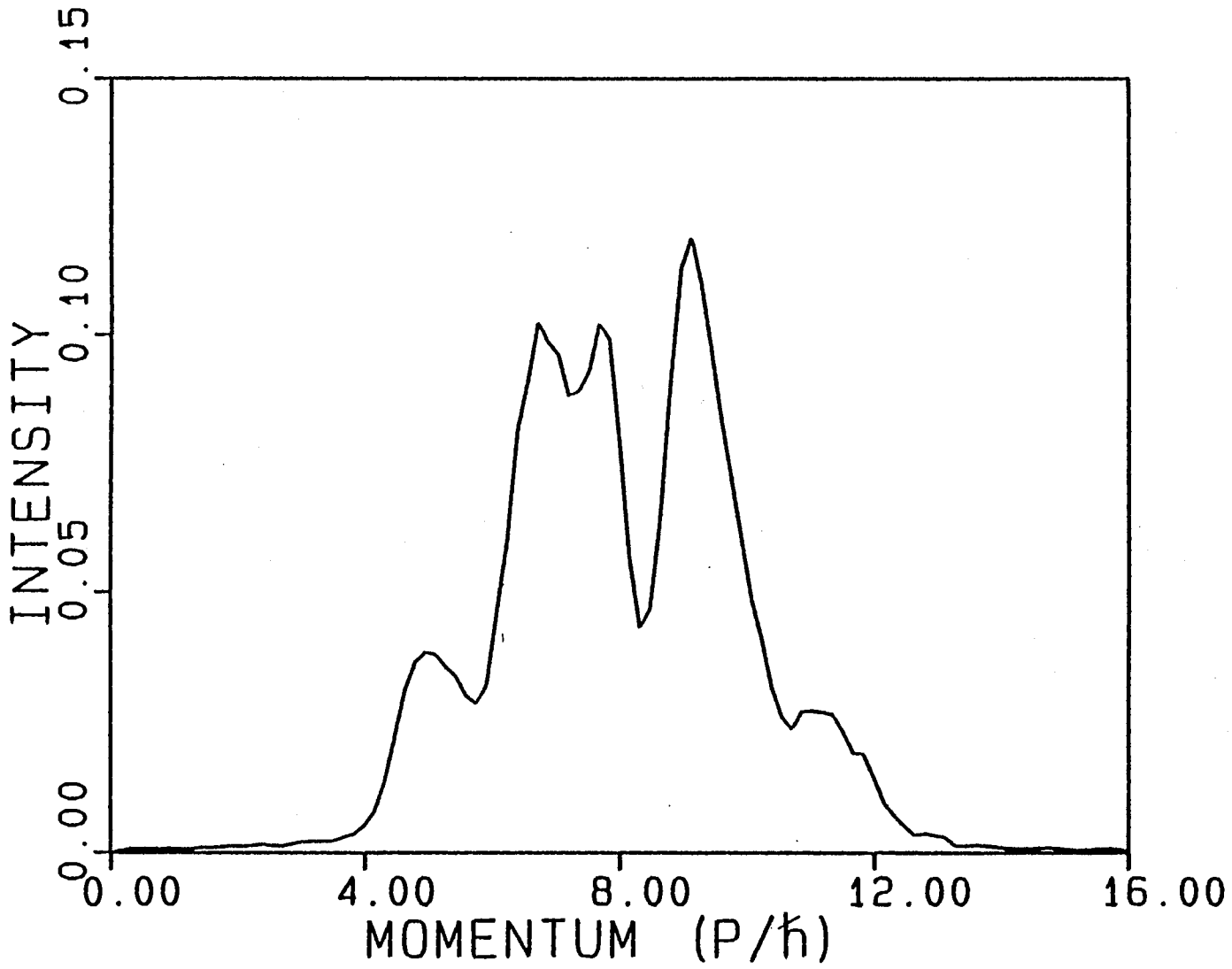

Figure 13. Final-State Momentum Distribution for Wave Packet at 45 Degree Incidence with Surface Motion in Mode 2 Parallel to the Incidnet Wave Vector

of the incident velocity vector is greater for 45 degree incidence.

An investigation into the effects of the surface Debye temperature on inelastic energy transfer was carried out. For all of the surface phonon mode studies, the surface vibrational force constant, fk, was 5.36 eV/Å^2. This force constant was varied by factors of 2 and 4 to study the effects on inelasticity. A lattice power spectrum is obtained by taking the Fourier transform of the motion of selected atom-atom bond lengths as a function of time. A combined power spectrum for the combined motion of the bond length between atoms 1 and 4 and the distance between a fixed atom below the surface plane and atom 2 is shown in Figure 14 with a spectrum resolution of 8 cm^{-1}. A combined spectrum for all the atom-atom distances would produce the entire range of frequencies exhibited by the lattice. Such a combined power spectrum was calculated for lattice force constants of 1.34, 2.68, 5.36, and 10.72 eV/Å^2. The frequencies produced were compared to the peak spacings in the final-state wave packet momentum distributions. The results of the comparisons are shown in Table IV. The correlation of the peak spacings with the lattice frequencies is seen to be excellent. Clearly, the scattered wave packet carries with it detailed information concerning the phonon spectrum of the lattice.

The calculations carried out to this point have involved a wave packet-lattice interaction potential represented by a pairwise sum of Lennard-Jones (6-12)

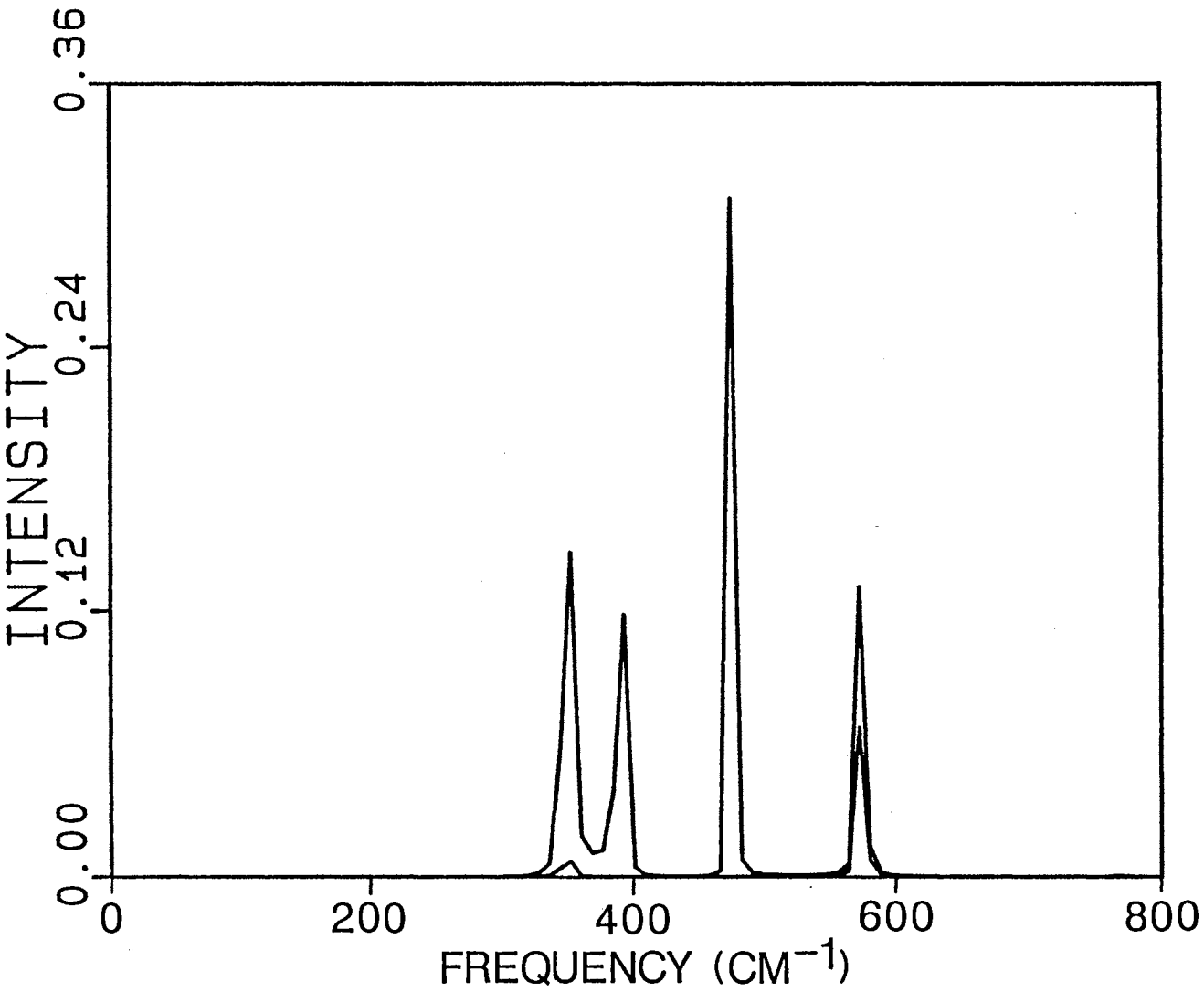

Figure 14. Lattice Power Spectrum for Motion of Atoms 1 and 4 and Motion between Atom 2 and a Fixed Atom

TABLE IV

LATTICE POWER SPECTRUM FREQUENCIES AND FINAL-STATE WAVE PACKET ENERGY SPACINGS FOR VARYING LATTICE FORCE CONSTANTS

Force constant ($eV/Å^2$)	(Lattice frequencies) x h (eV)		Wave packet energy spacings (eV)	
1.34	0.022	0.057	0.032	0.052
	0.036		0.037	
	0.043		0.043	
	0.048		0.048	
2.68	0.020	0.061	0.020	0.054
	0.031	0.068	0.022	
	0.041		0.030	
	0.051		0.041	
5.36	0.043		0.040	0.060
	0.049		0.044	0.067
	0.059		0.046	
	0.071		0.050	
10.72	0.061		0.063	
	0.100		0.104	

potentials given by Eq. (15). The parameters used produce a well-depth of -0.008731 eV at distance of 2.8 Å from the surface plane. An investigation of surface trapping and desorption requires that a somewhat arbitrary definition of surface trapping be utilized. The total integrated probability density of the wave function remaining within 7 Å of the surface plane is taken to be the total probability of adsorbed atoms. The evolution of the wave packet is continued as long as possible and the probability density is monitored. If we denote the maximum probability density within 7 Å of the surface as Po, the ratio of the total probability within this region to Po, P/Po calculated as a function of time gives the desorption rate. A plot of the ln[P/Po] vs time is shown in Figure 15 for values of the Lennard-Jones well-depth parameter $\epsilon = n\epsilon_o$ for n= 3, 5, and 7 with $\epsilon_o/k = 38.5$ K. Time is given in time units where 1 time unit is equal to 4.0×10^{-16}s. It can be seen that once desorption begins, the process is reasonably well described by a first-order rate law. The first-order rate coefficients for varying well depths were calculated from a least-squares fit of the linear portion of the decay curves in Figure 15. The results for varying well depths are given in Table V. As the well depth is increased, the rate at which the trapped atoms desorb from the surface would be expected to decrease. This is confirmed by data in Table V which shows a decrease in the first-order rate coefficients as the potential-energy well depth is increased over an order of magnitude.

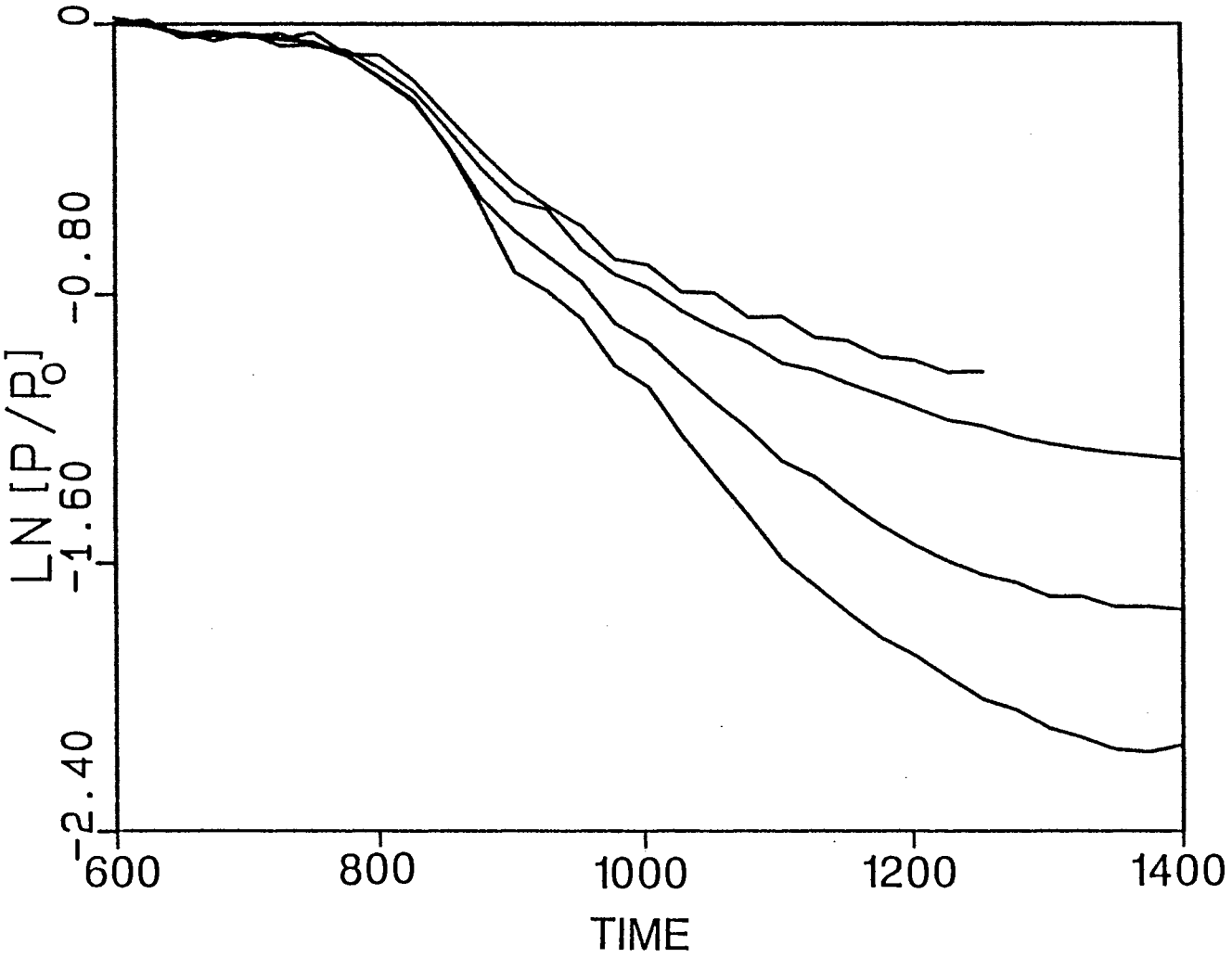

Figure 15. Ln(p/po) vs. Time for Differing Well-Depths

TABLE V

FIRST-ORDER DESORPTION RATE CONSTANTS FOR WAVE PACKET AT DIFFERENT WELL DEPTHS

Well depth (eV)	Rate coefficient (s^{-1}) (x 10^{-2})
0.02619	11.4-11.9
0.04366	9.15-9.56
0.06112	7.05-7.53
0.06548	6.81-7.35
0.06985	6.69-7.23
0.07421	6.64-7.20
0.07858	6.45-7.08
0.08294	6.18-6.77
0.08731	5.98-6.52

An effective temperature Te can be calculated using a simple Arrhenius rate law:

$$(35) \quad \ln[k_d] = \ln Q - E_w/RT_e$$

where k_d is the first-order rate constant, E_w is the potential-energy well depth, R is the gas constant and T_e is the effective temperature in degrees Kelvin. For an equilibrated system, the effective temperature should approach the surface temperature. A plot of $\ln[k_d]$ vs. well depth is given in Figure 16. The plot shows two linear portions, one below 0.06 eV, the other one above 0.06 eV. A least-squares fit to the portion of the plot greater than 0.06 eV yields an effective temperature of 1700 K. This is close to the surface temperature of 1500 K indicating that the longer residence times on the surface have allowed the system to equilibrate to a degree. The shallower well depths result in very short residence times as indicated by the region below 0.06 eV. The effective temperature in this region is about 800 K indicating much less thermal accommodation.

Perturbation-Trajectory Calculations

The development of the perturbation-trajectory method for the study of gas-surface inelastic scattering arose from the observation that in the NO-Ag(111) system, the mass of

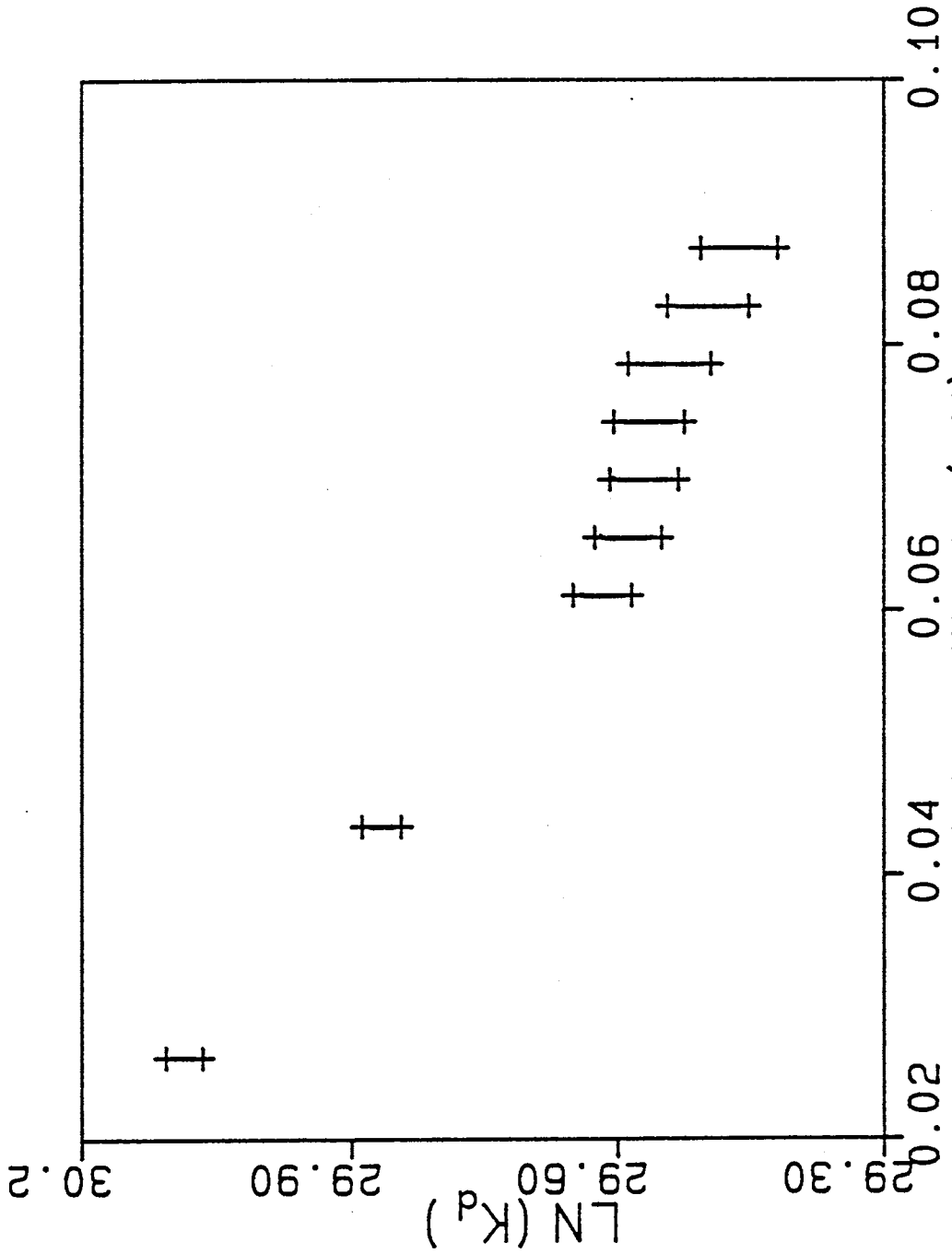

Figure 16. Variation of Ln(kd) vs. Well-Depth

the silver atoms is on the order of 12 times that of the incoming atoms. Consequently, with the very small gas atom/surface atom mass ratio of 0.1298, we might expect a NO collision with a Ag(111) surface to exert only minor perturbations upon the Q-zone trajectory. Under such conditions, the results obtained from a perturbation treatment should be nearly exact.

The surface used in these calculations consists of 68 silver atoms in three layers as described in Chapter II. The surface is shown in Figure 4. The open circles represent moving surface atoms, the closed circles represent moving atoms in the second layer. The squares designate nonmoving atoms in all three layers. The closed squares are atoms in the third layer, squares with crosses are atoms in the second layer, and the open squares designate nonmoving atoms in the first layer. The NO molecule is allowed to interact with the 14 moving surface atoms through the potential developed by Muhlhausen et at.[61] given in Eq.(22).

Initially, an exact classical calculation was done on this system by explicitly integrating the equations of motion of all 23 surface atoms along with those for the NO molecule. In the nomenclature of a perturbation calculation, this corresponds to assigning a 25-atom P-zone and a 45-atom B-zone. The translational energy distribution for the scattered molecules is given in Figure 17A. This is the result of 1000 scattered trajectories. The surface temperature is 650 K and the initial translational energy of the NO molecule is 96.48 kJ/mole. The initial NO rotational states

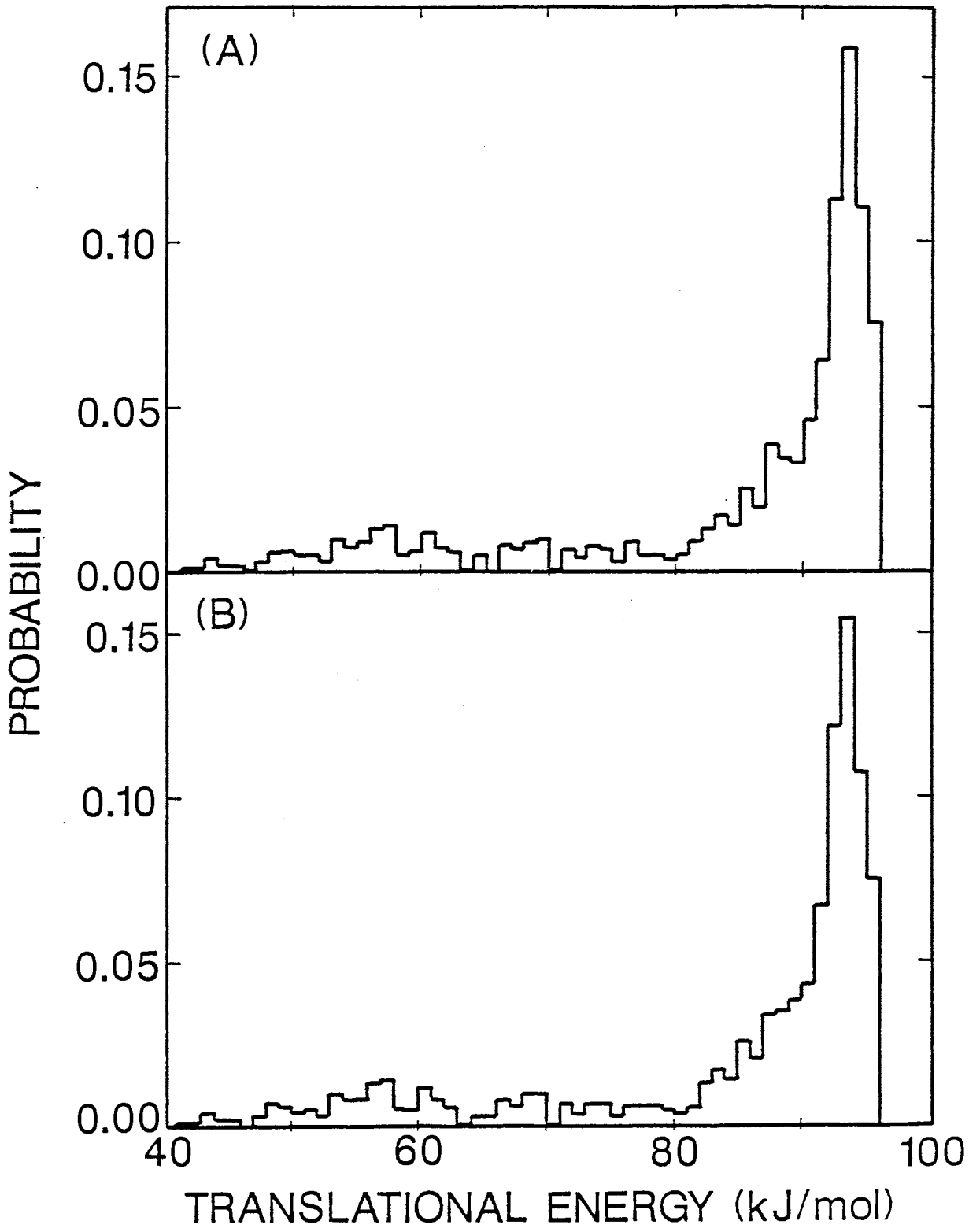

Figure 17. Translational Energy Distributions for NO Scattered from Ag(111)

were selected from a Boltzmann distribution at a rotational temperature of 20 K. Incident angles were selected from a cosine distribution. The distribution shows a great deal of elasticity corresponding to the most probable scattered energy being equal to the incident energy.

The perturbation calculation reassigns the P-zone to include the NO molecule only. The remaining 23 moving surface atoms are now included in the Q-zone. As described in Chapter II, the Q-zone trajectory is calculated and stored. The P-zone dynamics are then calculated in the time-dependent field generated by motion of the surface atoms. The translational energy distribution for 1000 trajectories with identical initial conditions as those used in the exact calculation is shown in Figure 17B. The results are nearly identical to the exact distribution shown in Figure 17A. These two distributions differ in their first and second moments by only 0.0014 and 2.41% ,respectively.

The in-plane spatial distributions for the exact and perturbation results are shown in Figures 18 and 19, respectively. The surface temperature is still 650 K and incidence angles are averaged over a cosine distribution. The rotational and translational energies are selected from Boltzmann distributions at 650 K. The angles are given in degrees. Again, comparison between exact results and those calulated using a two atom P-zone in the perturbation approximation shows excellent agreement.

The potential-energy surface utilized in all of these calculations was obtained from the work carried out by

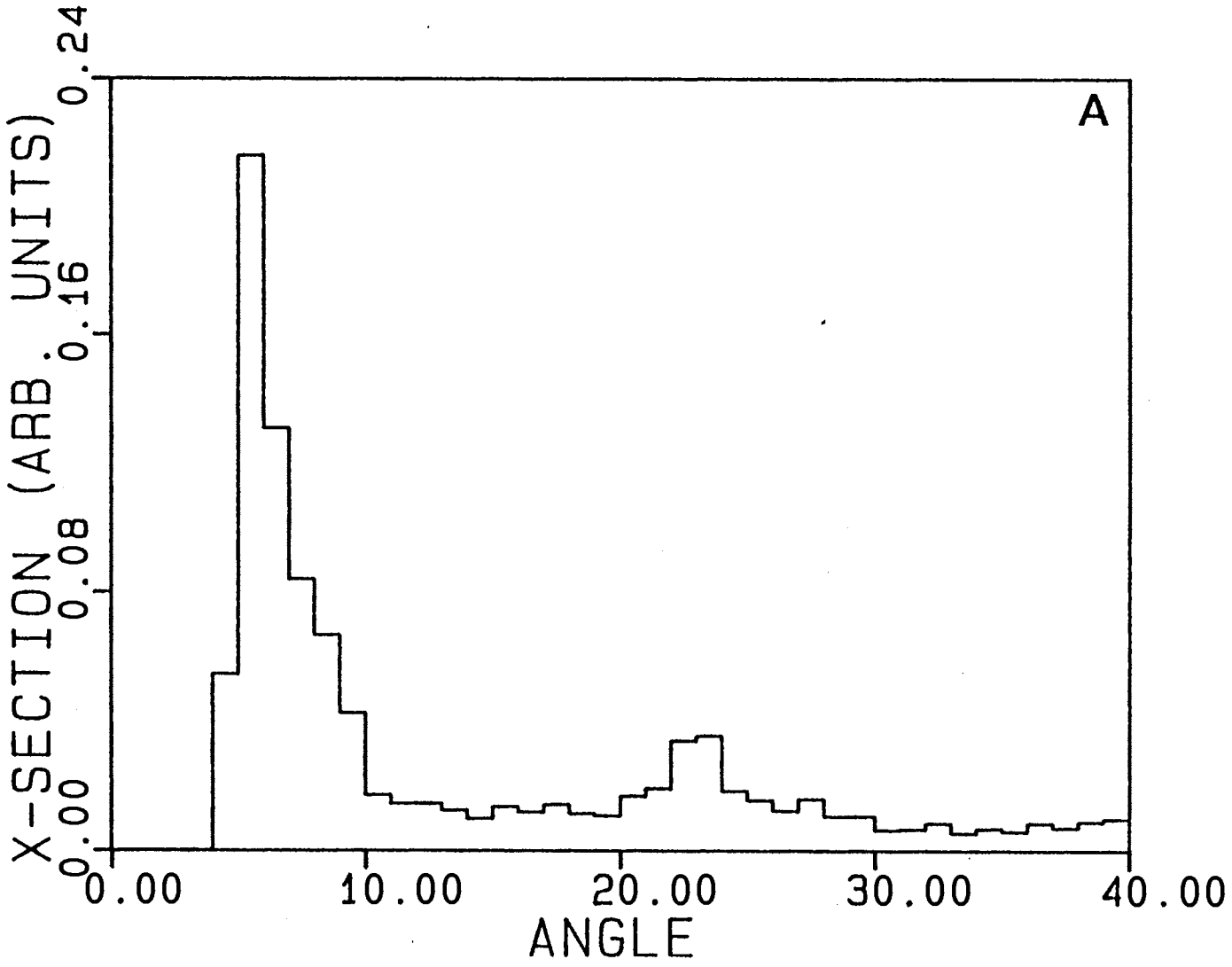

Figure 18. Perturbation Results of Differential Cross Section for NO Scattered from Ag(111)

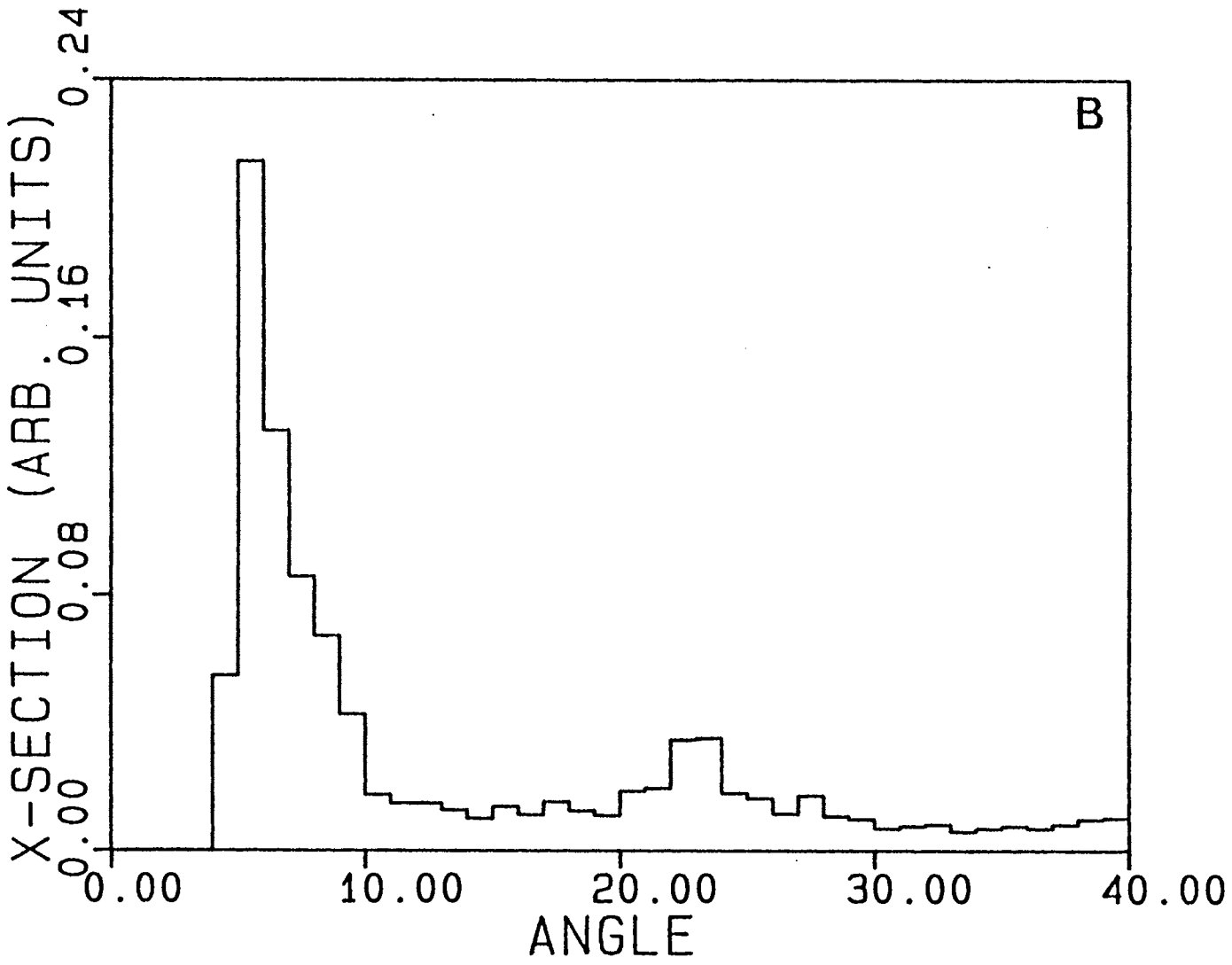

Figure 19. Exact Results of Differential Cross Section for NO Scattered from Ag(111)

Muhlhausen, Williams, and Tully[19]. In their work, the effect on the NO molecule by the Q-zone was determined using a Langevin ghost atom formalism[114]. This fact allows a convenient comparison of the exact, perturbation, and Langevin methods. The conditions in both studies are identical with one exception. In the study carried out by Muhlhausen et al., the number of atoms on the surface with which the NO molecule was allowed to interact is 14. However, only four of these lattice atoms were allowed to move. Since, in our calculations, all 14 surface atoms are in motion, the nature of the forces experienced by the incoming molecule will be somewhat different.

The rotational energy distributions for the exact, perturbation, and Langevin calculations are shown in Figure 20. The initial translational energy of the NO molecule is 96.48 eV. The initial rotational states were selected from a Boltzmann distribution at 20 K and the incident angle is 15 degrees relative to the surface normal. The open circles represent the result of 1000 trajectories using exact calculations. The diamonds are the results of the perturbation calculation and the triangles are the Langevin results reported by Muhlhausen et al.[19]. The perturbation results are seen to follow the exact results almost perfectly. All methods predict a linear decrease in the number of molecules with rotational-energy states up to 10 kJ/mol followed by a broad feature described by Kleyn et al.[41-44] as a "rotational rainbow". The Langevin results predict a higher probability of molecules at higher rotational states.

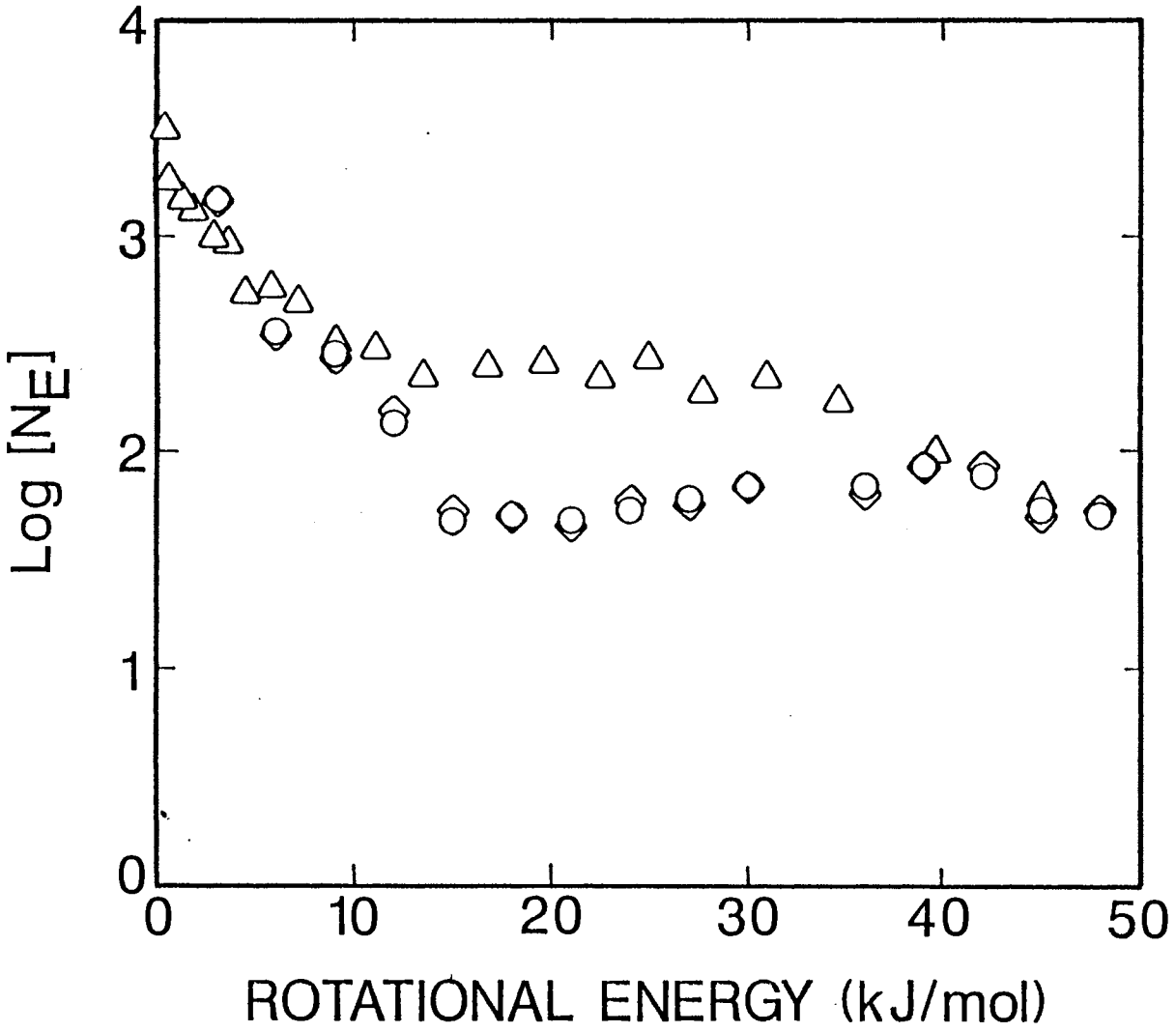

Figure 20. Rotational Energy Distributions for NO Scattered from Ag(111)

This is probably due to the differences in the forces experienced by the NO because of the additional moving atoms in the surface of this study. This is supported by results obtained with a model surface in which the entire surface was frozen. It was found that freezing the surface atoms provided a significant increase in the rotational energy distributions at higher rotational energies[122].

The sticking probabilities as a function of translational energy are given in Figure 21. The surface temperature is 750 K and the initial NO rotational energy is selected from a Boltzmann distribution at the surface temperature. Incident angles were selected from a cosine distribution. The perturbation results and the exact results provide virtually identical probabilities and are indicated by the stars. The squares are the results obtained from Muhlhausen et al. In this instance, there is no significant difference in any of the methods; however, the perturbation calculations provided a factor of 2.68 reduction in computer time from that required for the exact calculation.

Riley et al. have examined the capacity of the perturbation-trajectory method to act as a thermal reservoir. A surface composed of 666 krypton atoms in an fcc crystal was used. A 14-atom P-zone in the center of the crystal was given an initial temperature of 600 K. This P-zone was surrounded by a 158-atom Q-zone at a temperature of 300 K. The kinetic energy of the P-zone was then monitored over time. The kinetic energy was converted to

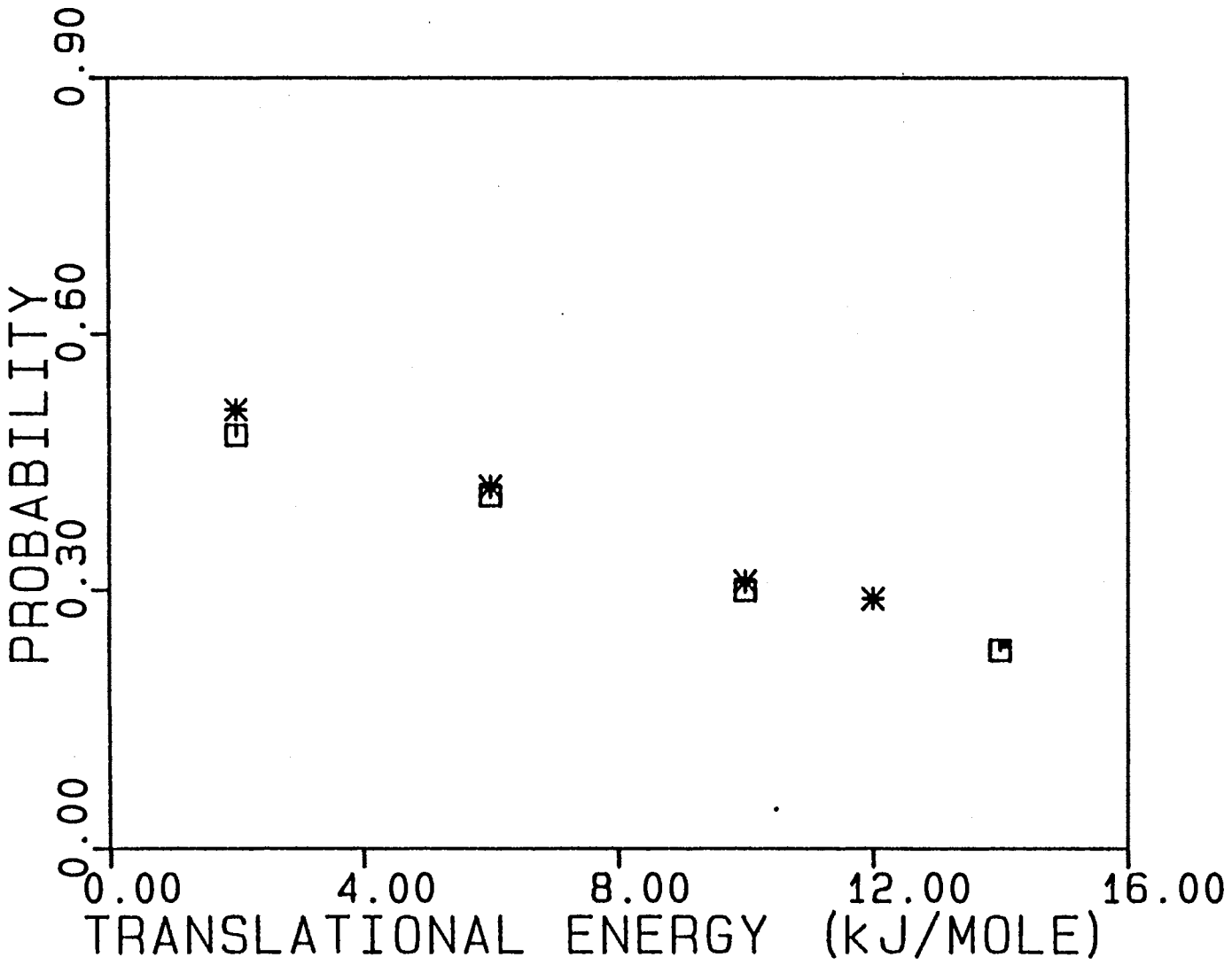

Figure 21. NO Sticking Probabilities vs. Incident Translational Energy for NO on Ag(111)

temperature using the expression E = 3nkT, where n = 14, k is the boltzmann constant and T is the temperature in degrees Kelvin. Since, on the average, one half of the total energy in the lattice system is in the form of kinetic energy, the P-zone atoms should equilibrate to a "kinetic energy" temperature of 150 K, if the system acts as an effective heat reservoir. It was found, however, that the temperature does not stabilize, but, in fact, increases indicating that the perturbation approximation is breaking down. When the P-zone is given no energy initially, and the Q-zone is given a temperature of 300 K, the P-zone is driven into motion as expected, however, no stabilization of temperature takes place.

The perturbation-trajectory method is seen then to be very accurate for short duration collisions, but fails to act as a heat sink or a heat reservoir. This is not surprising since at the heart of the perturbation method is the approximation that the Q-zone is unaffected by atoms contained within the P-zone. Atoms that have long residence times on the surface are unquestionably going to have significant effects on the rest of the surface particularly when the atoms are gaining kinetic energy from the surface or when the initial kinetic energy of the P-zone atoms is higher than that of the Q-zone atoms.

Reactions of Oxygen on Si(111)-(7x7)

In this section, the results of three sets of calculations carried out on the silicon(111)-(7x7)

reconstructed surface are presented. In the first set of calculations, oxygen atoms with 4.664 eV translational energy are scattered from the surface in order to determine the surface trapping probabilities. In the second study, the dynamics associated with molecular scattering of oxygen molecules is investigated, and finally, the dynamics of the silicon-oxygen system are examined under conditions in which one oxygen atom is allowed to interact with a surface containing an adsorbed oxygen atom. As discussed in the Introduction, these processes are all related to the phenomenon of "shuttle glow" in which 4.664 eV oxygen atoms are postulated to chemisorb upon a silica surface and undergo subsequent reaction with chemisorbed nitric oxide.

The potential-energy surface utilized for all these calculation is given in Chapter II. The surface features are given in Table VI. The Binnig et. al.[115] model for the silicon(111)-(7x7) surface used in this work contains 38 silicon atoms with dangling bonds. Twelve of these atoms are in the top layer of the surface while 26 atoms are approximately 1.5 a.u. below the upper surface plane (Figure 5). The binding energy for these two sites are given in Table VI. A contour map is given in Figure 22 for an oxygen atom in the (x,y) plane at a distance of 3.5 a.u. from the surface plane.

The results for oxygen atoms incident on the surface show the sticking probabilities to be very high for this system. For all trajectories, the incident energy of the incoming oxygen atom is taken to be 4.664 eV, which cor-

TABLE VI

POTENTIAL-ENERGY SURFACE FEATURES FOR OXYGEN ON Si(111)-(7x7)

Structural energies (eV)		Reference
Si-O (top site)	-3.4384	117
Si-O (bottom site)	-3.5224	117
O=O(g)	-5.0908	120
O-O(g)	-1.4738	117
Si-O-O-Si	-2.28	119
Si-O-O	-6.9199	118,119
Equilibrium Bond Lengths (a.u.)		
Si-O	3.8135	117,118
O=O(g)	2.2816	120
O-O(g)	2.7968	117
Stretching frequencies (cm^{-1})		
Si-O	485	117
O=O(g)	1580	120
O-O(g)	850	117
Bending frequencies (cm^{-1})		
Si-Si-O	370	117
Si-O-O	483	117

all structures are surface bound unless otherwise noted

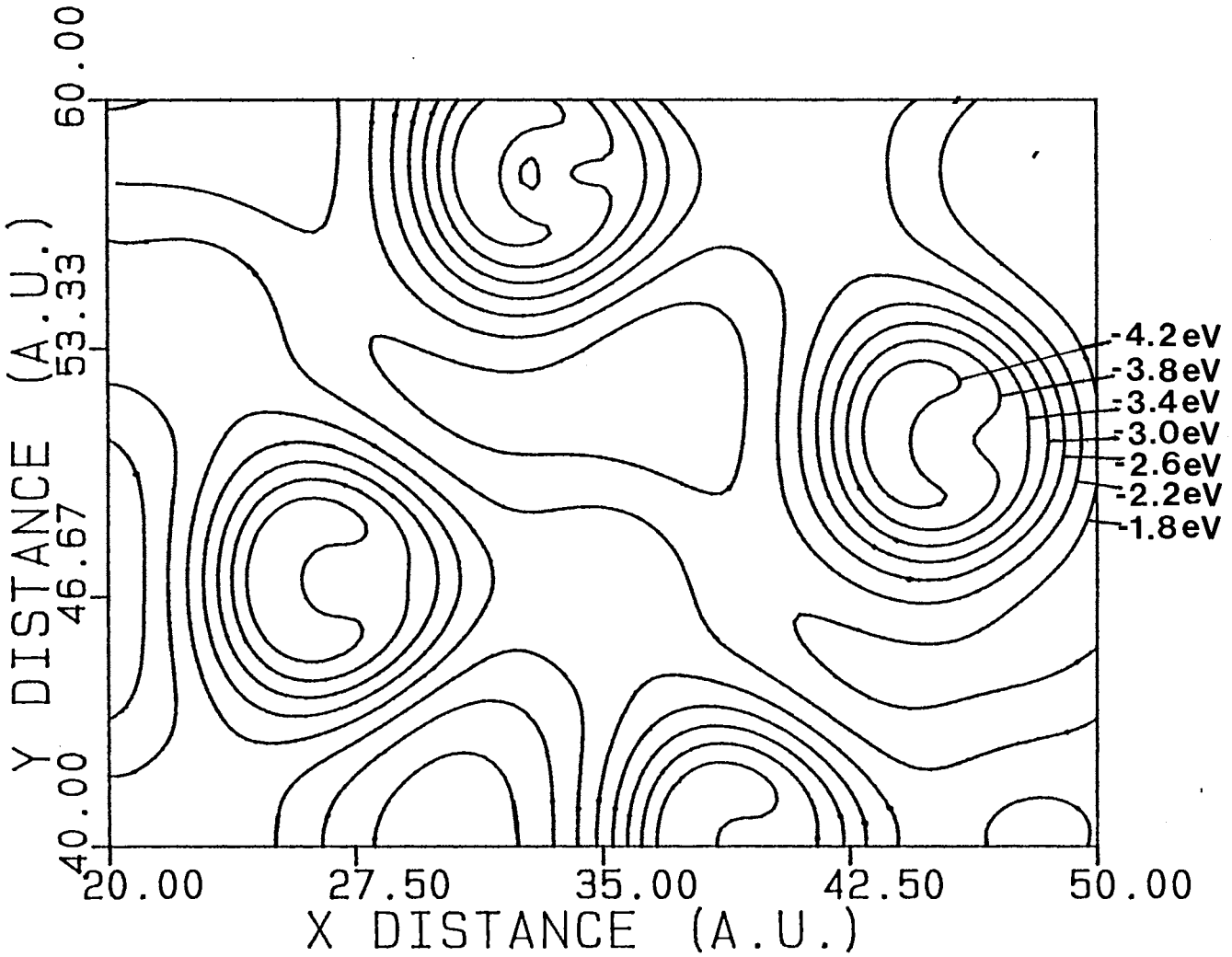

Figure 22. Contour Map for Oxygen Atom on Si(111)-(7x7)

responds to the average relative energy of a gas-surface collision between atmospheric particles and the forward (ram) surface of the shuttle orbiter at orbital velocities. The temperature of the surface was taken to be 300K. The average sticking probability was found to be 0.81 for oxygen atoms whose incident angle was selected from a cosine distribution. The target point on the surface was selected randomly. When the incident angle was selected from a sine distribution, the sticking probability was reduced to 0.68. The higher probability of sticking at incident angles closer to the surface normal is most probabably due to the bending terms introduced in the potential-energy surface to insure that the silicon-oxygen bond equilibrium position is normal to the surface plane. This type of result is not unexpected. It is generally found that energy transfer at the surface occurs primarily out of the perpendicular component of motion.

The variation of the distance from the surface plane with time for an oxygen atom trapped on the surface is shown in Figure 23. Distances are given in atomic units and one time increment is equivalent to 2.7×10^{-15} sec. The variation in kinetic and potential energies of the oxygen atom with time are shown in Figure 24. The incidence angle is 15.0 degrees from surface normal. These results show that the surface is able to sufficiently absorb enough energy during the high-energy collision to allow trapping and desorption studies to be done.

For the molecular system, the oxygen molecule changes

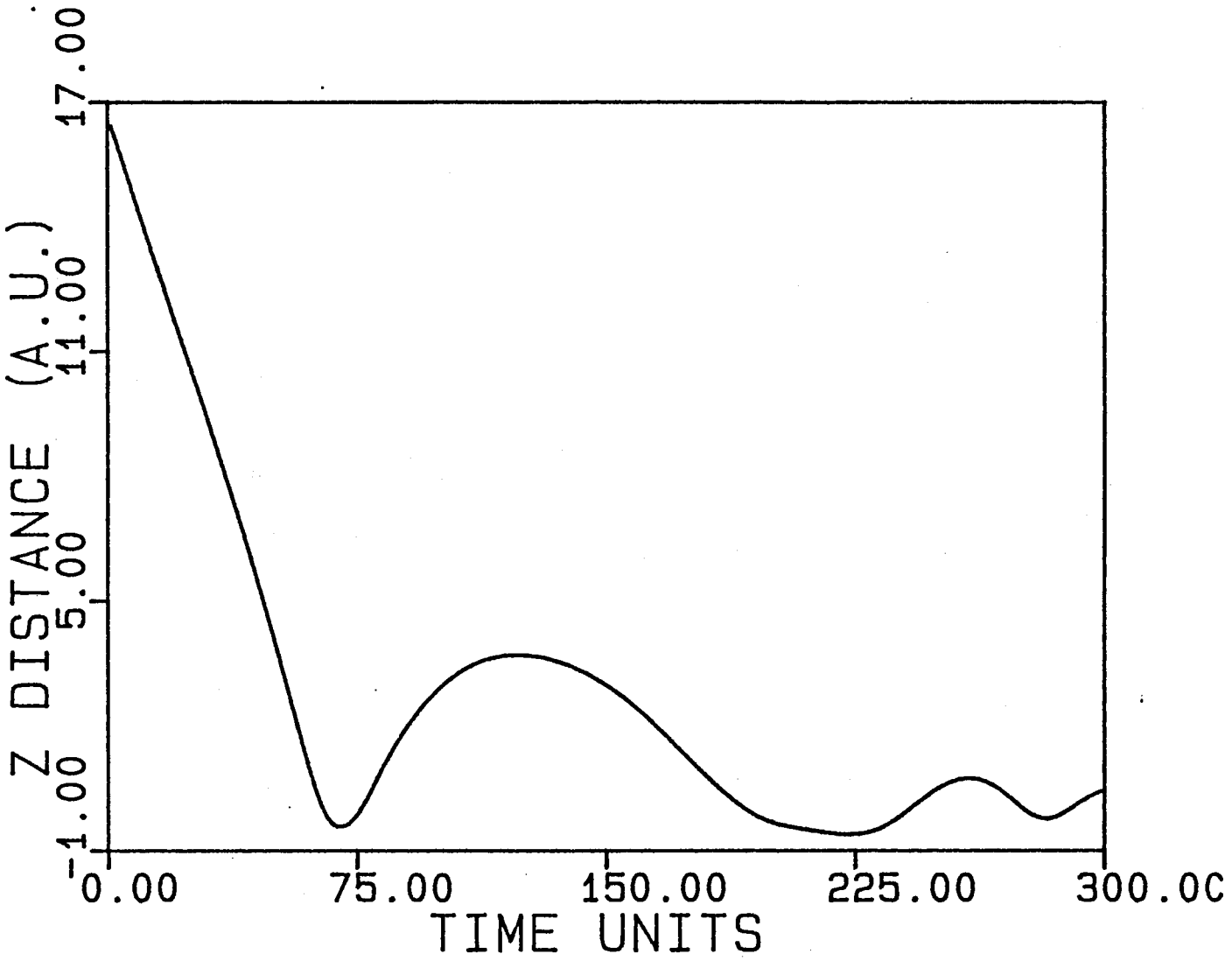

Figure 23. Perpendicular Distance of Oxygen Atom vs. Time for Trapped Trajectory

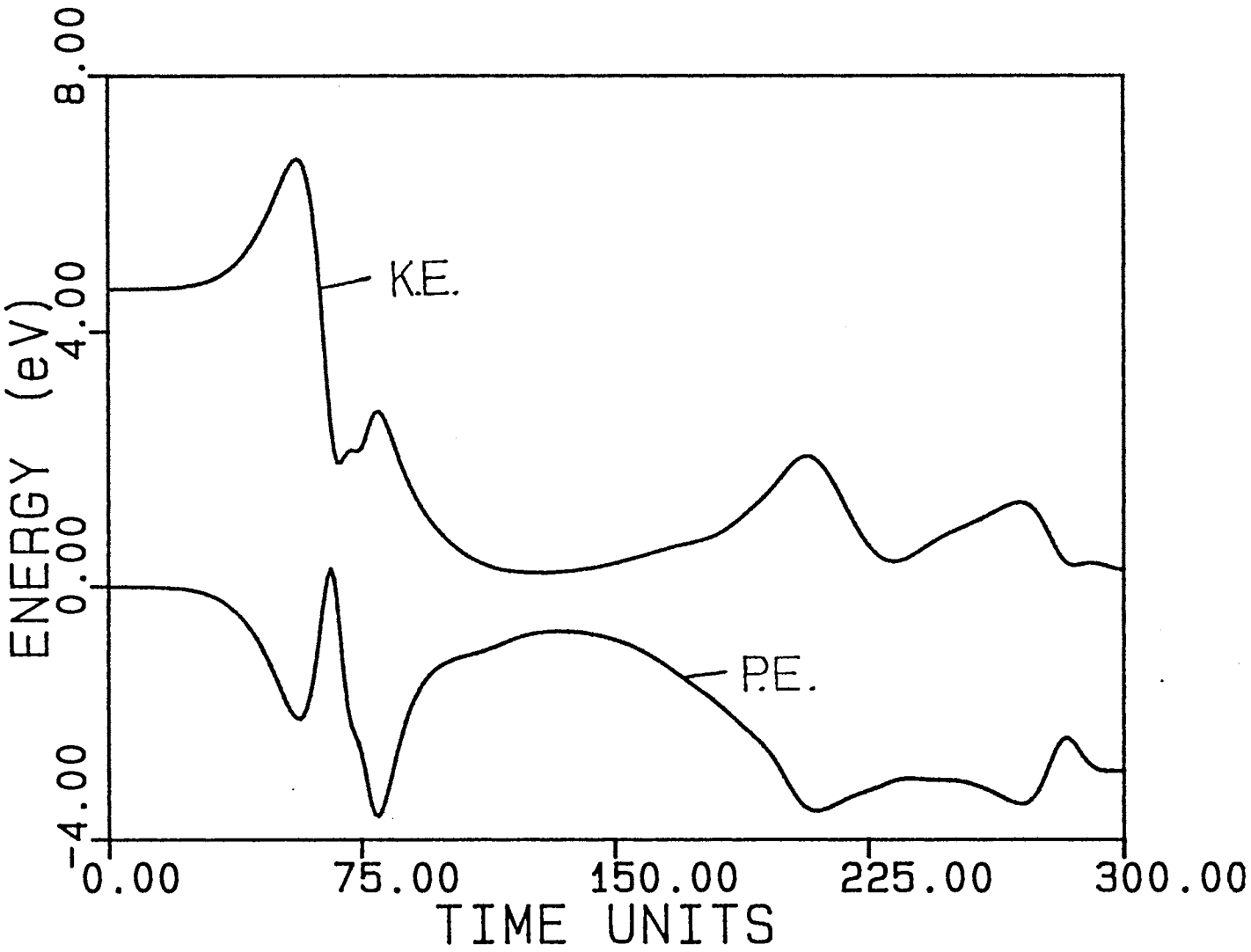

Figure 24. Variation in Kinetic and Potential Energies for Oxygen Atom Trapped Trajectory

from one with doubly-bonded character to a singly-bonded molecule. On this surface, as one end of the oxygen molecule binds to the unpaired electron of a silicon atom, the bonding in the oxygen molecule becomes intermediate between that of a double and single bond. Should the other end of the molecule bind to another silicon site forming a surface endoperoxide, the O_2 bond becomes that characteristic of a single bond. The possibility of a peroxide forming was found to be energetically unlikely. The average distance between closest silicon bonding sites in the (7x7) reconstruction is about 9.5 a.u. providing too great a distance between atoms for an effective peroxide to form. The energy of the peroxide structure is given in Table VI. When placed in this configuration, it was found that the structure is unstable and dissociates to two individual silicon-oxygen bonds. The presence of the Si-O-O structure on the surface was found to be energetically favorable and structurally stable. The energy of the Si-O bond plus the oxygens with "one and a half" bond character provide this stability. The energy and bending frequency for this configuration is given in Table VI.

The possible reaction channels after collision are

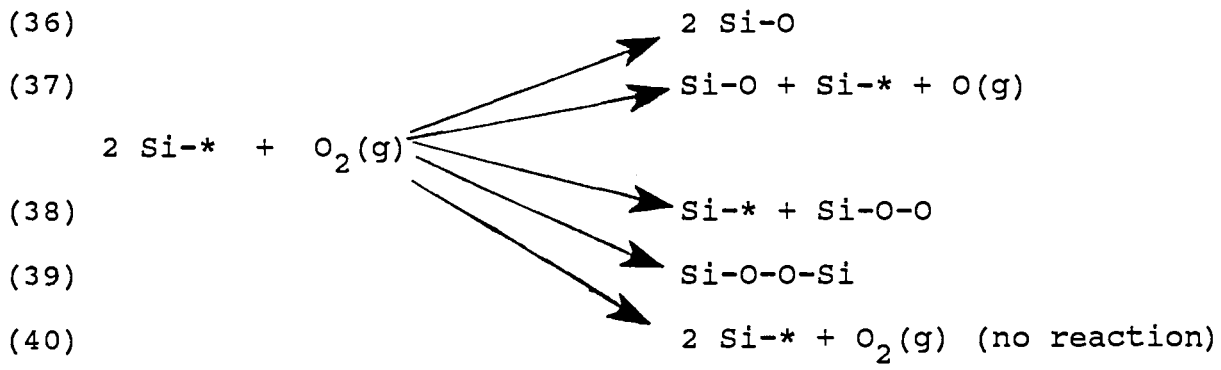

where Si-* denotes a surface dangling bond. All species are assumed to be surface bound unless otherwise noted. After one of these channels has occurred, other processes, such as surface migration and subsequent desorption, can take place due to the large amount of energy in the interaction region. Only the initial channels, (36)-(40), were examined in this work. The long term processes will be examined in greater detail in later work.

The results of 300 trajectories for the reaction system shown above are given in Table VII. All of the reaction channels shown were found to occur with the exception of the surface peroxide channel, Equation (39). This is due to the distance between the silicon atoms on this surface being too great to produce a sufficient stability for the peroxide. Reaction channel (38) was found to have a nearly 0.65 occurrence probability. The potential energy of this structure during examination of the potential-energy surface features shows this system to be extremely stable due to the strong bonding character of the oxygen-oxygen bond. The strong binding force between the two oxygens is also responsible for the frequent occurance of channel (40), (31%). On initial impact with the silicon surface, the high-energy collision appears to cause the oxygens to vibrate to near dissociation. The oxygen atoms are seen to quickly begin to equilibrate with the surface, which was observed to be reasonably efficient in the atomic oxygen scattering calculations, allowing them to reform molecular oxygen. However, when the collision is such that

TABLE VII

TRAJECTORY RESULTS FOR OXYGEN ON Si(111)-(7x7)

2 Si-*[a] + O_2(g) -->

Total number of trajectories = 300

Result	# of trajectories
2 Si-* + O_2(g)	93
Si-* + Si-O-O	193
Si-O + Si-O	10
Si-* + Si-O + O(g)	4

Si-* + Si-O + O(g) -->

Total number of trajectories = 375

Result	# of trajecories
Si-* + Si-O + O(g) (Oxygen exchange)	182
Si-O + Si-O	130
Si-* + Si-* + O_2	42
Si-* + Si-O-O	21

a Si-* denotes a surface dangling bond.

all structures are surface bound unless otherwise noted

the oxygens are scattered apart to larger distances, the surface atomic binding processes in equations (36) and (37) are found to take place. A plot of the oxygen-oxygen and the silicon-oxygen radial distances as a function of time for reaction channel (38) is shown in Figure 25. The plot of the oxygen-oxygen radial distance is raised by three atomic units for purposes of visual clarity. It is evident that after initial collision, the oxygen molecule stretches close to the dissociation limit and then returns and settles above a silicon bonding site. This is in contrast to Figure 26, which shows the oxygen molecule dissociating and both oxygen atoms bonding with open silicon sites. The distance between bonding sites is approximately 25 a.u. apart. In both figures, distances are in atomic units and time is in time units where one time unit is equal to 2.16×10^{-15} seconds. In Figure 26, it is seen that the oxygen molecule strikes the surface, stretches to near dissociation, and then undergoes one more vibrational turning point before dissociating.

Of particular interest, is the possibility of the recombination of oxygen atoms into oxygen molecules. Such a recombination would produce electronically excited states which could then decay producing visible light. When one of the oxygen atoms is replaced with NO, such a process is one possible source of the observed shuttle glow. The studies above show that oxygen atoms and molecules are easily captured by the silicon surface, justifying the presence of oxygen atoms on the surface. The next step is to examine

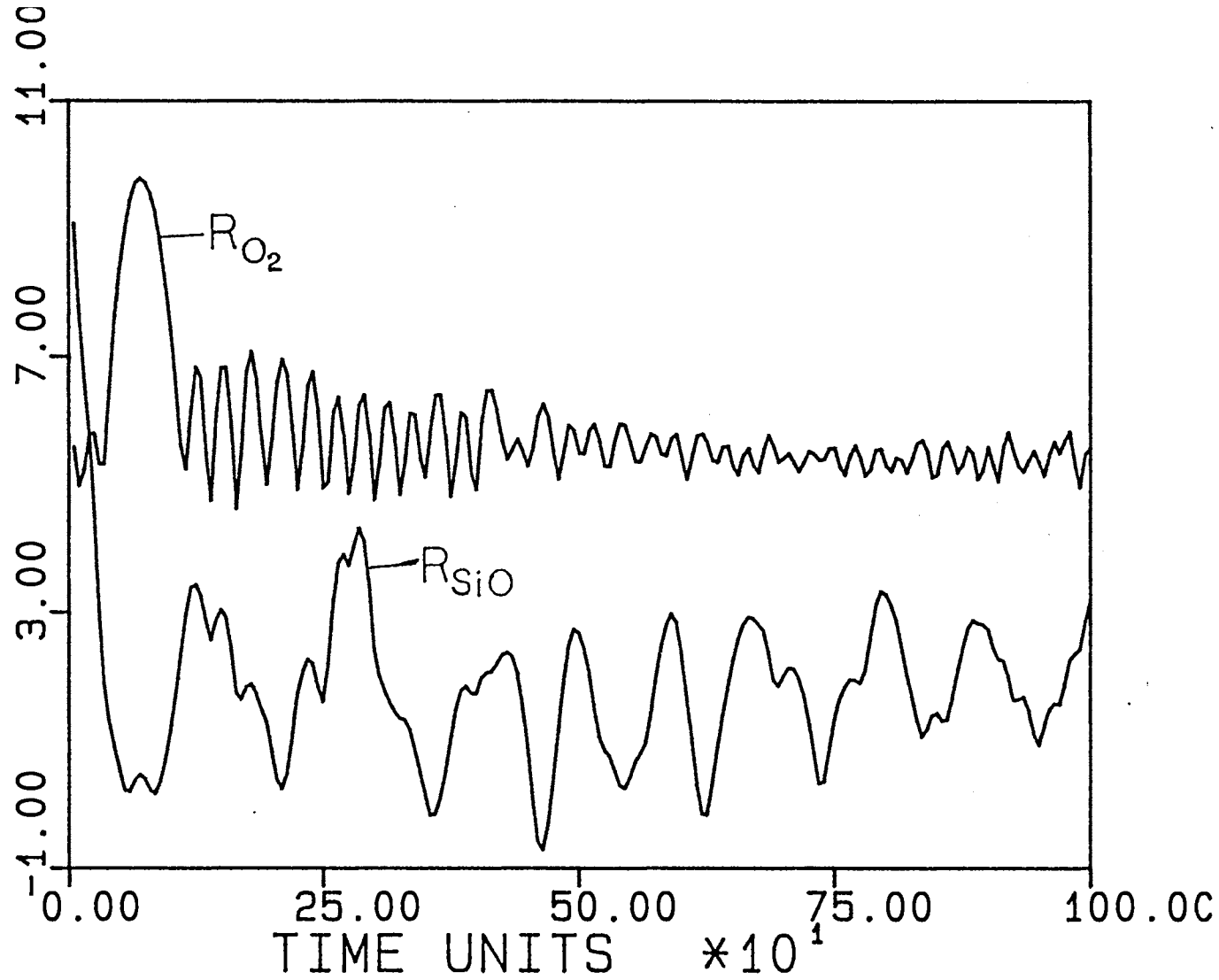

Figure 25. Variation of Oxygen-Oxygen Radial Distance and Silicon-Oxygen Radial Distance with Time for Reaction Channel 38

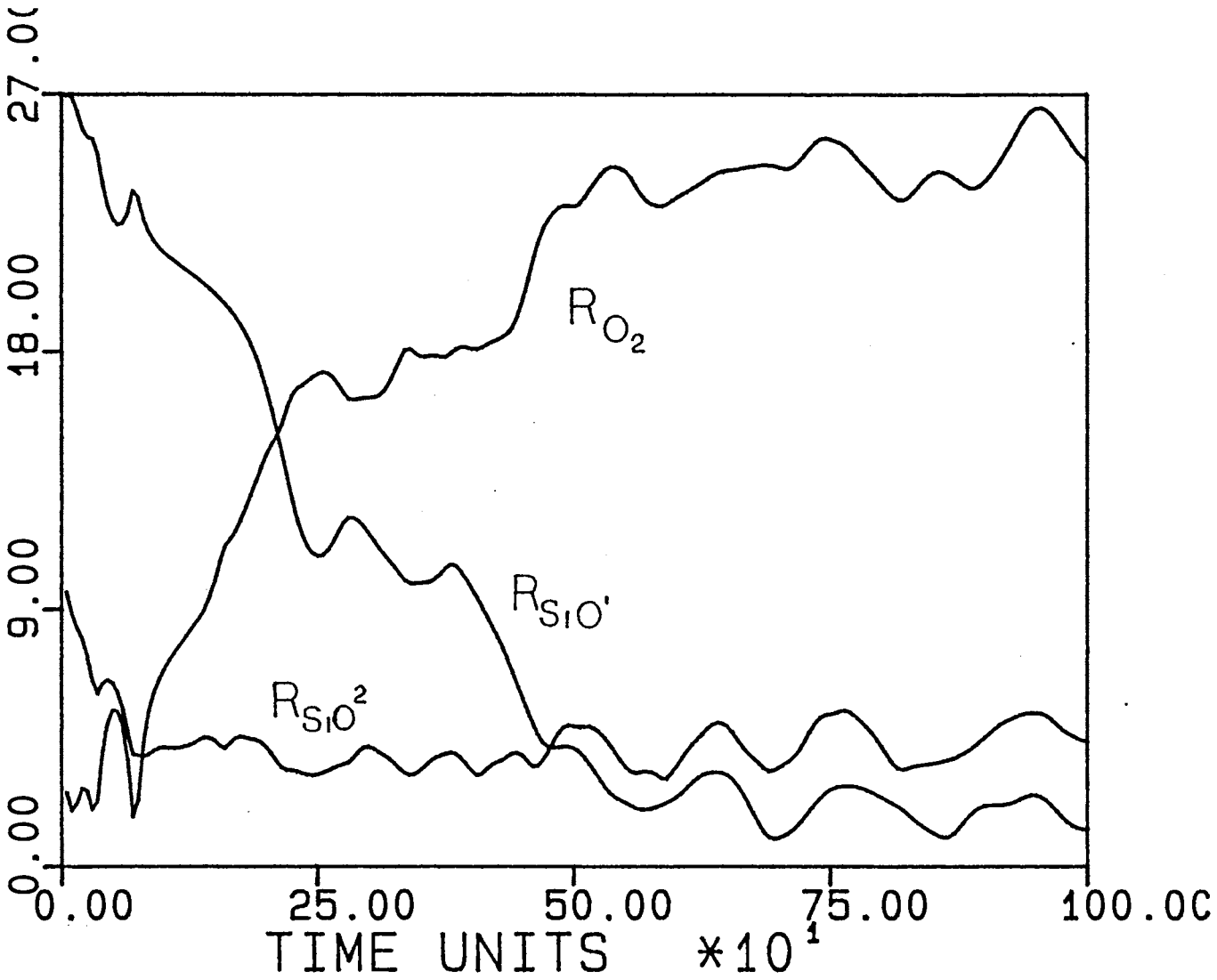

Figure 26. Variation of Oxygen-Oxygen Radial Distance and Silicon-Oxygen Radial Distance with Time for Reaction Channel 36

the dynamics of oxygen atom collisions with surfaces containing chemisorbed oxygen atoms. The possible reaction channels for this system are

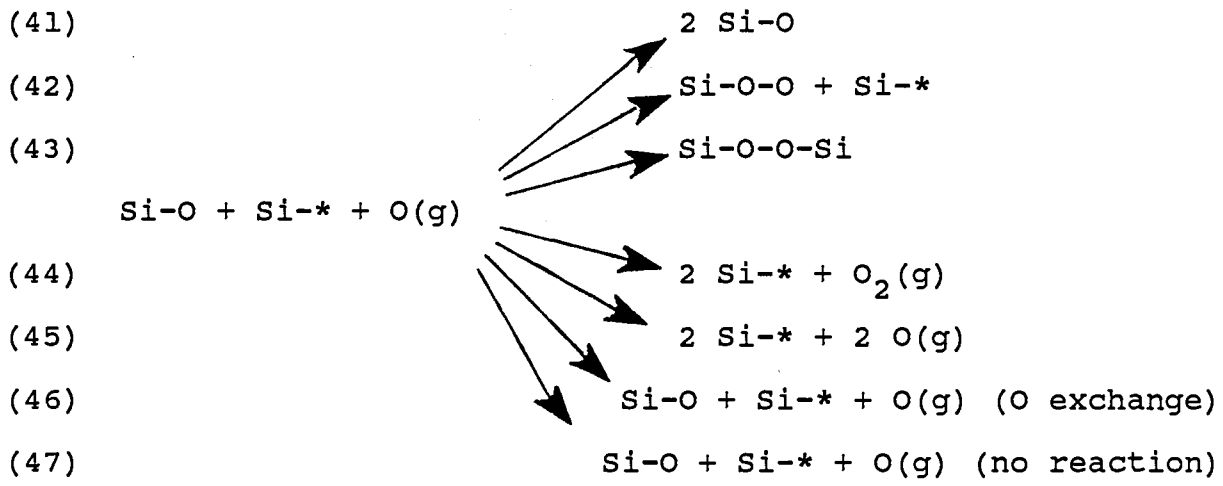

where Si-*, again, denotes a surface dangling bond. All species are assumed to be surface bound unless otherwise noted. Reaction channel (43) was not observed for the reasons discussed above. Reaction channel (45) requires that the oxygen-oxygen dissociation energy of 5.0908 eV be produced. Although there is a great deal of energy in this system, this reaction channel is not seen.

The results of 375 trajectories for this reaction system are given in Table VII. Of interest in this system was the interaction of the oxygen atoms, therefore, the aiming point incoming oxygen atom on the surface was selected randomly within a 5 a.u. by 3 a.u. rectangular surface area with the larger side of the area being oriented in the x direction and the smaller side directed in the y direction. As the collision point with the surface moves

farther from this area, the reaction dynamics approach that of a single oxygen atom scattering, as expected. Surprisingly, reaction channel (47) was not observed. This is probably due to this selection of initial aiming points for the incoming oxygen atom. More investigation into this result is being carried out. For all calculations in this system, the incoming angle of the incident oxygen atom was selected from a cosine distribution with an initial translational energy of 4.664 eV. The surface bound oxygen is placed in its equilibrium position directly above a silicon atom dangling bond site and allowed to move in thermal equilibrium with the surface at a temperature of 300 K.

Figure 27 shows an example of reaction channel (46). This reaction channel was found to have a relatively high occurance probability of 0.48 under the initial conditions specified. Figure 27 is a plot of the oxygen distance perpendicular to the surface plane vs. time where one time unit is equal to 2.7×10^{-15} seconds. Also included is the oxygen-oxygen radial distance. The oxygen-oxygen distance has been translated upward by 5 atomic units for visual clarity. All reactions of this channel involve the incoming high-energy oxygen atom colliding with the surface bound oxygen atom, moving close enough to become repulsive, and then dissociating the previously surface bound oxygen atom.

Reaction channel (41) was found to have an occurance probability of 0.35. In each of these events, the oxygen atoms are never close enough to become repulsive. The

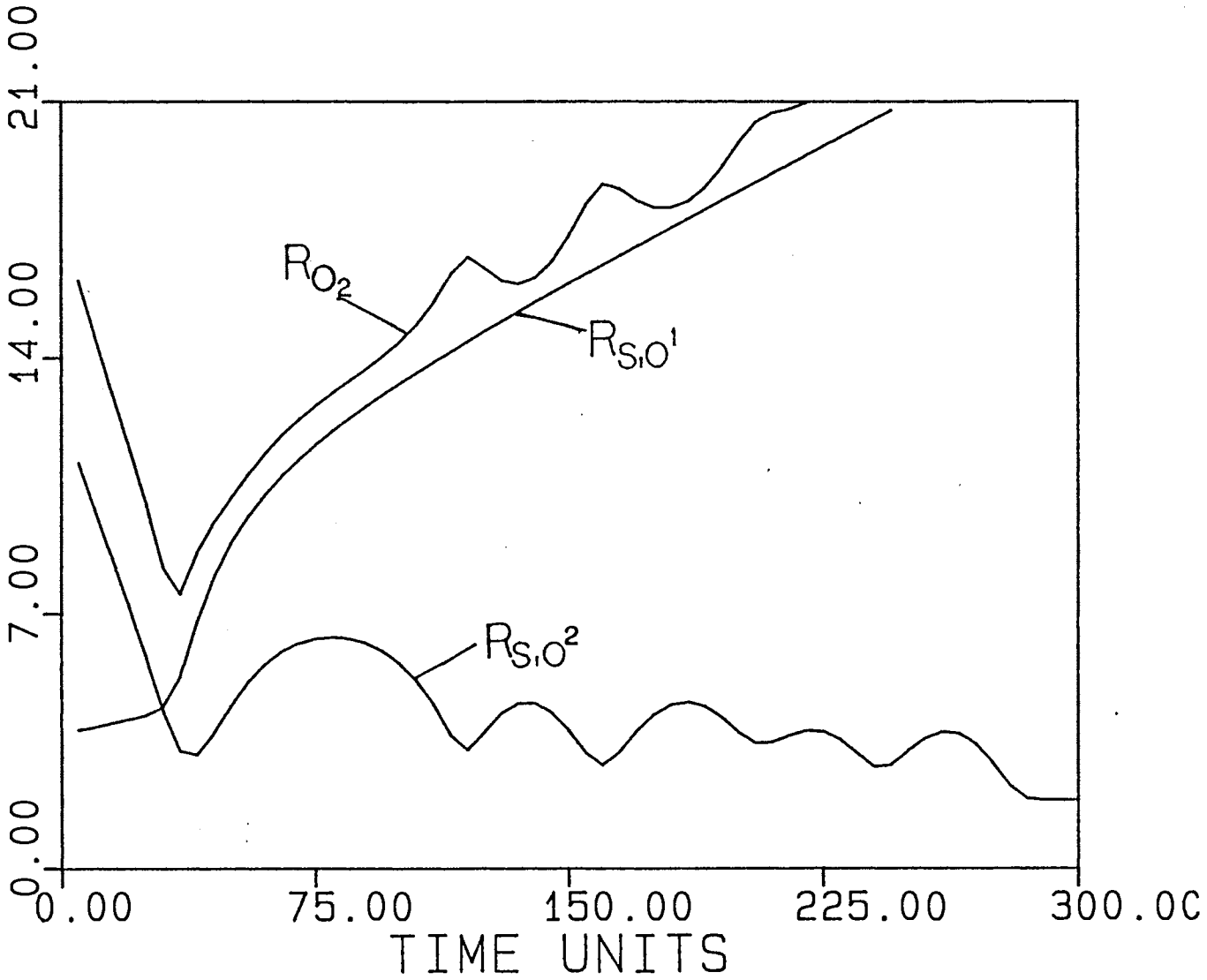

Figure 27. Variation of Oxygen-Oxygen Radial Distance and Silicon-Oxygen Radial Distance with Time for Reaction Channel 47

reaction most often occurs when the collision point of the incident oxygen atom on the surface is closer to the perimeter of the designated aiming area, thus the oxygen atoms never collide as the surface traps the incoming oxygen first. In effect, this channel is essentially that of an oxygen atom striking a clean surface. Less frequently, the surface oxygen is found to scatter in a manner similar to that observed for channel (46), however, the scattering angle is very large relative to surface normal and the oxygen is subsequently trapped by the surface. An example of this mechanism is shown in Figure 28 which shows the perpendicular distances of the oxygens with time along with the oxygen-oxygen radial distance. The oxygen-oxygen distance is increased by 5 for visual clarity. As is shown, both oxygens remain on the surface, but the scattered oxygen is initially driven away and then is "caught" by a silicon bonding site.

The reaction channel involving the recombination of oxygen atoms into oxygen molecules is of great interest and is represented by reaction (44). An example of this process is shown in Figure 29 which shows the scattered oxygen molecule as being in highly excited rotational and vibrational states. The amplitude of vibration brings the molecule to near dissociation limits. Although not represented in this calculation, it is reasonable to conclude that excited electronic states would also result which would then relax to the ground electronic state through radiative processes. It is these type processes

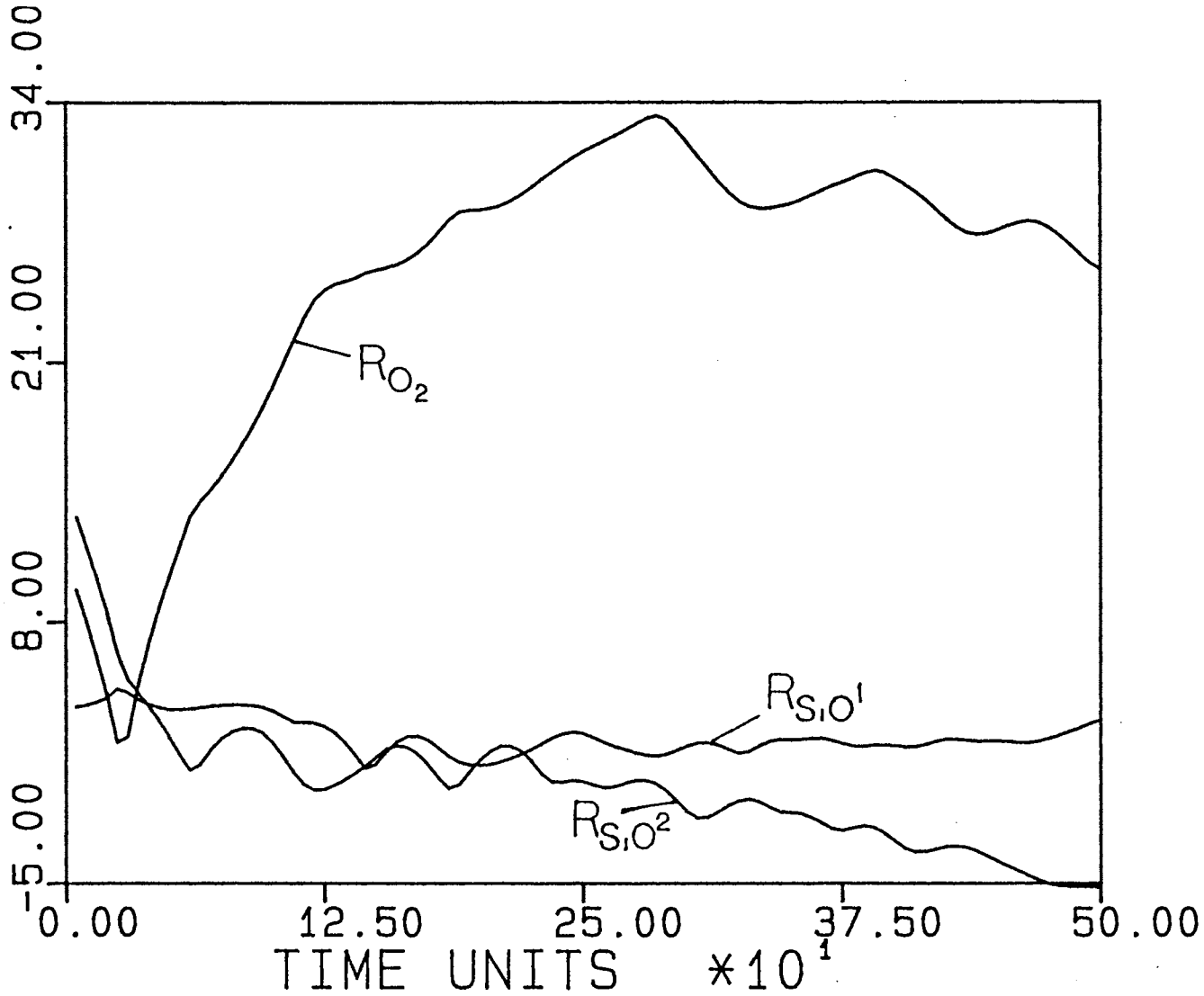

Figure 28. Variation of Oxygen-Oxygen Radial Distance and Silicon-Oxygen Radial Distance with Time for Reaction Channel 41

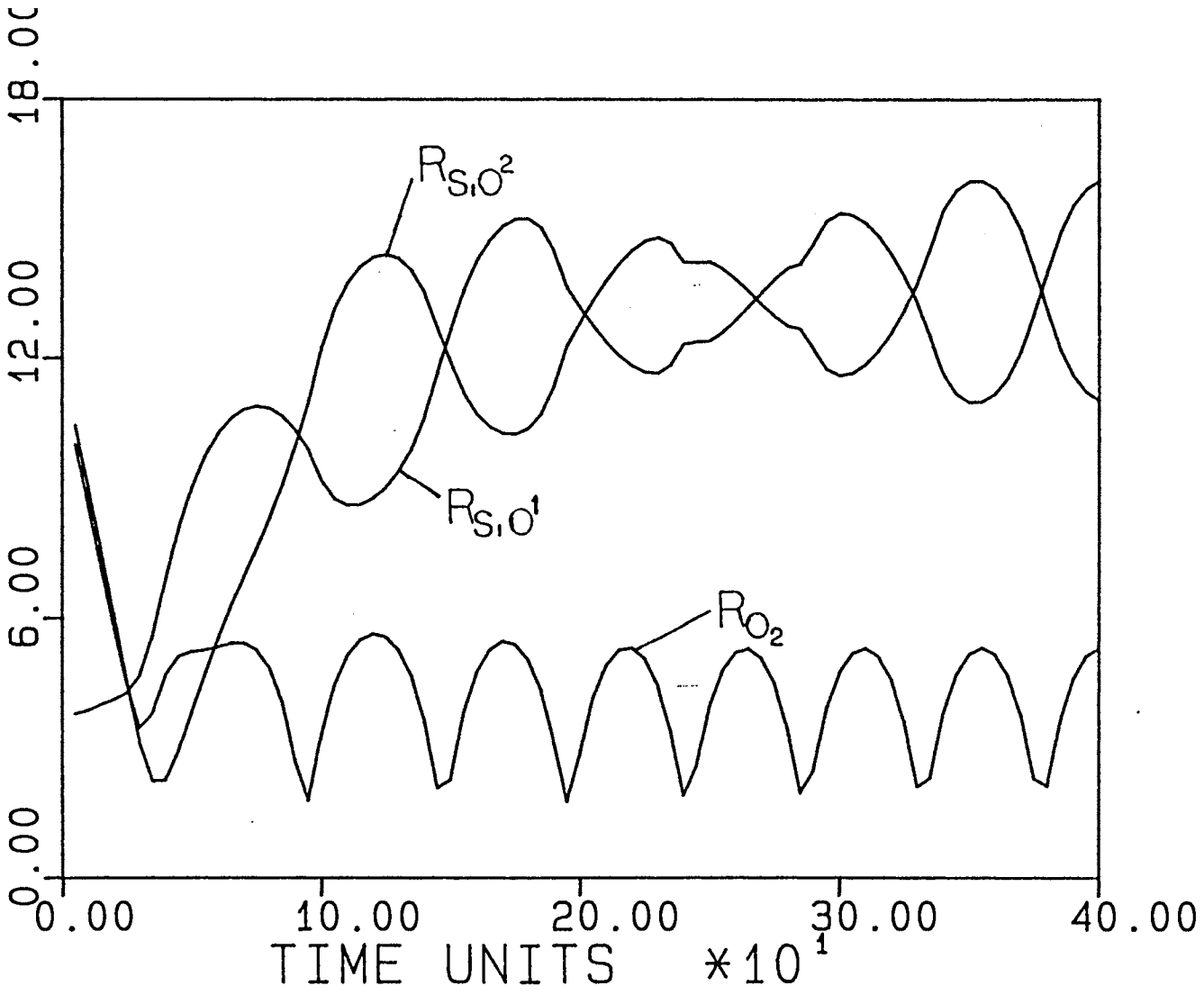

Figure 29. Variation of Oxygen-Oxygen Radial Distance and Silicon-Oxygen Radial Distance with Time for Reaction Channel 42

that are of principle interest. It was also found that channel (42) is very closely related. An example of this process is shown in Figure 30. Common to both of these reactions is that the incoming oxygen is intermediate between that of colliding with the surface-bound oxygen atom causing its dissociation, and being too far away from the surface atom to break the silicon-oxygen bond and being trapped by the silicon surface. In both channels, the incoming oxygen atom approaches the adsorbed oxygen atom to near the equilibrium bond length of oxygen molecules, about 2.5 atomic units. If it approaches too closely, the oxygen-oxygen interaction becomes repulsive and the atoms scatter away from each other as was found in the examination of reaction (41). The total recombination probability for channels (42) and (44) of 0.17 indicate that the region between oxygen atom scattering and oxygen atom adsorption is fairly narrow. The integration step size utilized in this calculation prevents accurate determination of the size of this impact region. Channel (42) producing the surface peroxide results from very similar mechanisms as observed in channel (44) with the exception that the resulting oxygen molecule does not have enough translational energy to escape the surface attractive forces and is subsequently trapped. None of the products of peroxide formation were seen to dissociate into two silicon-oxygen bonds, however, long time behavior of adsorbed species was not examined.

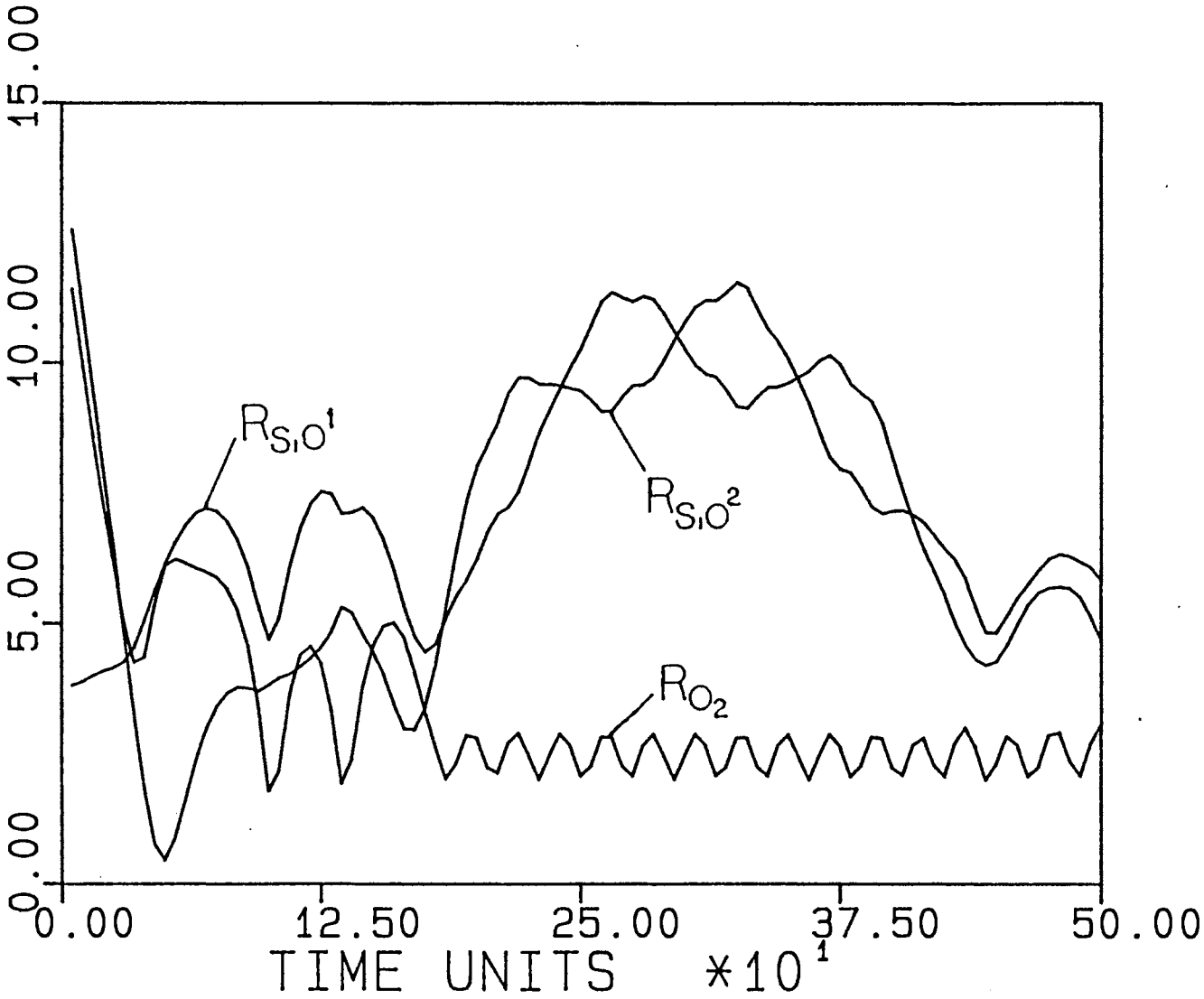

Figure 30. Variation of Oxygen-Oxygen Radial Distance and Silicon-Oxygen Radial Distance with Time for Reaction Channel 44

CHAPTER IV

CONCLUSIONS

Wave packet Trajectory Studies

A Semiclassical wave packet formulation has been used to determine the relative importance of different surface vibrational surface modes and the surface Debye temperature on inelastic scattering. Also, first-order rate coefficients were calculated from the variation of the "adsorbed" wave packet probability density as a function of potential-energy well depth.

From examination of the 27 surface phonon modes associated with a nine-atom lattice, it was found that energy transfer to and from the lattice surface occurs when lattice atoms in the surface impact region contain a momentum component in the direction of the wave packet momentum vector. For conditions in which there was no motion in the impact region, or in which the motion of the lattice atoms were were perpendicular to the motion of the incident wave packet, very little or no energy transfer was seen to take place.

Excellent correlation between the lattice power spectrum and the peak separations in the final-state energy

distributions of scattered wave packets was observed. A change in the surface Debye temperature results in a corresponding change in the collision inelasticity.

The desorption rate for the wave packet system was seen to decrease as the surface potential-energy well depth was increased. The rate was found to follow a first-order rate law for shallow well depths. For larger potential wells, a smaller slope in a first-order rate law was observed. Calculation of the nominal surface temperature shows greater thermal accomodation for larger well depths.

Perturbation-trajectory method

A perturbation-trajectory method was introduced for the purposes of the reduction in computer time in the calculation of the gas-surface collisional dynamics. This method partitions the system into a primary P-zone, a Q-zone and in some cases, a stationary B-zone. The labels follow those employed by the generalized Langevin approach to reactive scattering. In the perturbation approximation, the particles in the Q-zone are assumed to be unaffected by the dynamics in the P-zone. Within this approximation, the positions and momenta of the Q-zone atoms can be determined at all times and used to generate a time-varying potential field in which the dynamics of the P-zone can be determined.

The perturbation-trajectory approach was applied to the NO-Ag(111) system. For this system, the NO gas molecule is designated as the P-zone and a surface composed of 23 moving atoms was designated as the Q-zone. The low gas-atom

to surface-atom mass ratio is expected to result in excellent agreement with "exact" calculations in which the dynamics of the entire system are considered without perturbation approximation. The results show this to be the case. The energy and scattering angle distributions of scattered trajectories were found to agree almost exactly with those calculated from a full 25-atom P-zone. Comparison to the results calculated from the identical system using a generalized Langevin approach are found to be good to excellent. Differences in final rotational energy distribution were observed and attributed to a reduced number of moving atoms utilized in the Langevin approach.

Scattering of Oxygen from a Si(111)-(7x7) surface

An investigation into the dynamics of oxygen atom and oxygen molecule scattering at orbital velocities from a Si(111)-(7x7) reconstructed surface was carried out in order to gain insight into the mechanism associated with the observance of the shuttle glow phenomena. Three levels of calculation were studied. The surface trapping probabilities for this surface were determined by the scattering of atomic oxygen. The dynamics of oxygen molecule scattering were then studied, followed by the scattering of oxygen atoms from a surface containing an adsorbed oxygen atom present.

Trapping probabilities for oxygen atoms incident on the silicon reconstruction were found to be very high and were seen to increase as the incident angle approached a

vector normal to the surface plane. The surface was found to effectively dissipate the high incident momenta of the oxygen atoms.

Investigation of molecular scattering showed a large fraction of surface peroxide structures. A silicon-oxygen molecule surface endoperoxide was found to be energetically unlikely due to the large interatomic lattice distances. A large fraction of molecules were found to scatter from the surface unreacted. About 3% of the integrated molecular trajectories were found to dissociate on the surface.

The dynamics of the oxygen atom scattering from a surface containing an adsorbed oxygen atom produced several possible reaction channels. Predominant is the exchange of oxygens on the surface. This mechanism was found to occur for cases in which there was a direct collision between the oxygen atoms. For larger impact parameters, the incident oxygen atom was seen to adsorb on the surface without affecting the previously adsorbed atoms, as was expected. For intermediate impact parameters, the oxygen atoms are found to combine into oxygen molecules and scatter if enough energy has not been dissipated into the surface. If the molecules do not contain enough energy to escape, surface peroxides are observed to form.

This work represents an introduction into the investigation of the mechanisms associated with the shuttle glow phenomena. Future work is necessary, inevitable and will involve the introduction of nitrogen species as diatomic nitric oxide and nitrogen, and triatomic nitrous

oxide and nitrogen dioxide. A study into each of these systems and their related mechanisms is expected to deliver extremely useful insight into this and other gas-surface systems.

REFERENCES

1. E. A. McCullough Jr. and R. E. Wyatt, J. Chem. Phys. 51 (1969) 1253.

2. E. A. McCullough Jr. and R. E. Wyatt, J. Chem. Phys. 54 (1971) 3578.

3. G. E. Kellerhals, N. Sathyamurthy, and L. M. Raff, J. Chem. Phys. 64 (1976) 818.

4. P. M. Agrawal and L. M. Raff, J. Chem. Phys. 74 (1981) 5076.

5. P. M. Agrawal, N. C. Agrawal, R. Viswanathan, and L. M. Raff, J. Chem. Phys. 80 (1984) 760.

6. P. M. Agrawal and L. M. Raff, J. Chem Phys. 77 (1982) 3946.

7. C. B. Smith, L. M. Raff, and P. M. Agrawal, J. Chem Phys. 83 (1985) 1411.

8. G. Drolshagen and E. J. Heller, J. Chem. Phys. 82 (1895) 226.

9. G. Drolshagen and E. J. Heller, Surface Sci. 139 (1984) 260.

10. G. Drolshagen and E. J. Heller, J. Chem. Phys. 79 (1983) 2072.

11. R. Kosloff and C. Cerjan, J. Chem Phys. 81 (1984) 3722.

12. R. B. Gerber, A. T. Yinnon, and R. Kosloff, Chem. Phys. Lett. 105 (1984) 523.

13. A. T. Yinnon and R. Kosloff, Chem. Phys. Lett. 102 (1983) 216.

14. E. J. Heller, J. Chem. Phys. 62 (1975) 1544.

15. E. J. Heller, Chem. Phys. Lett. 34 (1975) 321.

16. E. J. Heller, J. Chem. Phys. 64 (1976) 63.

17. M. J. Davis and E. J. Heller, J. Chem. Phys. 71 (1979) 3383.

18. N. De Leon and E. J. Heller, J. Chem. Phys. 78 (1983) 4005.

19. E. J. Heller, J. Chem. Phys. 65 (1976) 4979.

20. R. C. Mowery and D. J. Kouri, Chem. Phys. Lett. 119 (1985) 285.

21. B. Jackson and H. Metiu, J. Chem. Phys. 84 (1986) 3535.

22. A. Askar and A. S. Cakmak, J. Chem. Phys. 68 (1978) 2794.

23. H. Tal-Ezer and R. Kosloff, J. Chem. Phys. 81 (1984) 3967.

24. H. F. Harmuth, J. Math. and Phys. 36 (1957) 269.

25. D. Kosloff and R. Kosloff, J. Comp. Phys. 52 (1983) 35.

26. R. Bisseling and R. Kosloff, J. Comp. Phys. 59 (1985) 136.

27. R. M. Lambert and C. M. Comrie, Surface Sci. 46 (1974) 61.

28. J. L. Gland, Surface Sci. 71 (1978) 327.

29. J. L. Gland and B. A. Sexton, Surface Sci. 94 (1980) 355.

30. T. H. Lin and G. A. Somorjai, Surface Sci. 107 (1981) 573.

31. R. J. Gorte and L. D. Schmidt, Surface Sci. 109 (1981) 367.

32. W. L. Guthrie, T. H. Lin, S. T. Ceyer, and G. A. Somorjai, J. Chem. Phys. 76 (1982) 6398.

33. M. Asscher, W. L. Guthrie, T. H. Lin, and G. A. Somorjai, J. Chem. Phys. 78 (1983) 6992.

34. M. Asscher, W.L. Guthrie, T. H. Lin, and G. A. Somorjai, Phys. Rev. Lett. 49 (1982) 76.

35. J. Segner, H. Robota, W. Vielhaber, G. Ertl, F. Frenkel, J. Hager, W. Krieger, and H. Walther, Surface Sci. 131 (1983) 273.

36. F. Frenkel, J. Hager, W. Krieger, H. Walther, C. T. Campbell, G. Ertl, H. Kuipers, and J. Segner, Phys. Rev. Lett. 46 (1981) 152.

37. C. T. Campbell, G. Ertl, and J. Segner, Surface Sci. 115 (1982) 309.

38. D. A. Mantell, R. R. Cavanaugh, and D. S. King, J. Chem. Phys. 84 (1986) 5131.

39. H. Ibach and S. Lehwald, Surface Sci. 76 (1978) 1.

40. C. M. Comrie, W. H. Weinberg, and R. M. Lambert, Surface Sci. 57 (1976) 619.

41. A. W. Kleyn, A. C. Luntz, and D. J. Auerbach, Surface Sci. 117 (1982) 33.

42. A. W. Kleyn, A. C. Luntz, and D. J. Auerbach, Phys. Rev. Lett. 47 (1981) 1169.

43. A. C. Luntz, A. W. Kleyn, and D. J. Auerbach, Phys. Rev. B 25 (1982) 4273.

44. A. C. Luntz, A. W. Kleyn, and D. J. Auerbach, J. Chem. Phys. 76 (1982) 737.

45. G. M. McClelland, G. D. Kubiak, H. G. Rennagel, and R. N. Zare, Phys. Rev. Lett. 46 (1981) 831.

46. P. J. Goddard, J. West, and R. M. Lambert, Surface Sci. 71 (1978) 447.

47. H. Asada and T. Matsui, Jap. J. Appl. Phys. 21 (1982) 259.

48. H. Asada, Jap. J. Appl. Phys. 20 (1981) 527.

49. G. D. Kubiak, J. E. Hurst, H. G. Rennagel, G. M. McClelland, and R. N. Zare, J. Chem Phys. 79 (1983) 5163.

50. G. McElhiney, H. Papp, and J. Pritchard, Surface Sci. 54 (1976) 617.

51. R. M. Logan and R. E. Stickney, J. Chem. Phys. 44 (1966) 195.

52. J. D. Doll, J. Chem. Phys. 59 (1973) 1038.

53. W. L. Nichols and J. H. Weare, J. Chem. Phys. 62 (1975) 3754.

54. W. L. Nichols and J. H. Weare, J. Chem. Phys. 66 (1977) 1075.

55. J. E. Hurst, G. D. Kubiak, and R. N. Zare, Chem. Phys. Lett. 93 (1982) 235.

56. A. W. Kleyn, A. C. Luntz, and D. J. Auerbach, Surface Sci. 152 (1985) 99.

57. J. A. Barker, A. W. Kleyn, and D. J. Auerbach, Chem. Phys. Lett. 97 (1983) 9.

58. J. G. Lauderdale, J. F. McNutt, and C. W. McCurdy, Chem. Phys. Lett. 107 (1984) 43.

59. E. Zamir and R. D. Levine, Chem. Phys. Lett. 104 (1984) 143.

60. J. C. Polanyi and R. J. Wolf, J. Chem. Phys. 82 (1985) 1555.

61. C. W. Muhlhausen, L. R. Williams, and J. C. Tully, J. Chem. Phys. 83 (1985) 2594.

62. J. A. Barker and D. J. Auerbach, Surf. Sci. Rep. 4 (1985) 1.

63. J. C. Tully and M. J. Cardillo, Science 223 (1984) 445.

64. J. C. Tully, Acc. Chem. Res. 14 (1981) 188.

65. G. Pirug, H. P. Bonzel, H. Hopster, and H. Ibach, J. Chem. Phys. 71 (1979) 593.

66. E. K. Grimmelman, J. C. Tully, and E. Helfand, J. Chem. Phys. 74 (1981) 5300.

67. S. Anderson and J. Harris, Phys. Rev. B 27 (1983) 9.

68. A. Modl, T. Gritsch, F. Budde, T. J. Chang, and G. Ertl, Phys. Rev. Lett. 57 (1986) 384.

69. D. S. King and R. R. Cavanaugh, J. Chem. Phys. 76 (1982) 5634.

70. F. Frenkel, J. Hager, W. Krieger, H. Walther, G. Ertl, J. Segner, and W. Vielhaber, Chem Phys. Lett. 90 (1982) 225.

71. H. D. Meyer and R. D. Levine, J. Chem. Phys. 80 (1983) 189.

72. J. C. Tully, Surface Sci. 111 (1981) 461.

73. F. O. Goodman, Surface Sci. 3 (1965) 386.

74. H. Voges and R. Schinke, Chem. Phys. Lett. 100 (1983) 245.

75. H. Voges and R. Schinke, Chem. Phys. Lett. 95 (1983) 221.

76. J. A. Serri, J. C. Tully, and M. J. Cardillo, J. Chem. Phys. 79 (1893) 1530.

77. A. C. Diebold and G. Wolken Jr., Surface Sci. 82 (1979) 245.

78. G. Wolken Jr., J. Chem. Phys. 58 (1973) 3047.

79. G. Wolken Jr., J. Chem. Phys. 59 (1973) 1159.

80. A. M. Richard and A. E. Depristo, Surface Sci. 134 (1983) 338.

81. A. E. Depristo, Surface Sci. 137 (1984) 130.

82. S. Y. Lee and E. J. Heller, J. Chem. Phys. 76 (1982) 3035.

83. S. Sawada, R. Heather, B. Jackson, and H. Metiu, J. Chem. Phys. 83 (1985) 3009.

84. V. Mohan and N. Sathyamurthy, Curr. Sci. 55 (1986) 115.

85. S. A. Lebedeff, Phys. Rev. 165 (1968) 1399.

86. R. H. Bisseling, R. Kosloff, and D. Kosloff, Comp. Phys. Comm. 39 (1986) 313.

87. M. W. Jezercak, C. B. Smith, L. M. Raff, and P. M. Agrawal, J. Chem Phys. 88 (1988) 1264.

88. P. M. Banks, P. R. Williamson, and W. J. Raitt, Geo. Res. Lett. 10 (1983) 118.

89. S. B. Mende, R. Nobles, P. M. Banks, O. K. Garriott, and J. Hoffmann, Geo. Res. Lett. 21 (1984) 374.

90. M. R. Torr, Geo. Res. Lett. 10 (1983) 114.

91. G. R. Swenson, S. B. Mende, and K. S. CLifton, Geo. Res. Lett. 12 (1985) 97.

92. B. D. Green, G. E. Caledonia, and T. D. Wilkerson, J. Spacecraft. 22 (1985) 500.

93. S. B. Mende, G. R. Swenson, K. S. Clifton, R. Gause, L. Leger, and O.K. Garriot, J. Spacecraft. 23 (1986) 189.

94. I. L. Kofsky, Geo. Res. Lett. 15 (1988) 241.

95. J. H. Yee, V. J. Abreu, and A. Dalgarno, Geo. Res. Lett. 12 (1985) 651.

96. R. H. Prince, Geo. Res. Lett. 12 (1985) 453.

97. B. D. Green, Geo. Res. Lett. 11 (1984) 576.

98. T. G. Slanger, Geo. Res. Lett. 10 (1983) 130.

99. G. R. Swenson and R. E. Meyerott, Geo. Res. Lett. 15 (1988) 245.

100. J. H. Yee and V. J. Abreu, Geo. Res. Lett. 10 (1983) 126.

101. S. R. Langhoff, R. L. Jaffe, J. H. Yee, and A. Dalgarno, Geo. Res. Lett. 10 (1983) 896.

102. S. B. Mende, O. K. Garriott, and P. M. Banks, Geo. Res. Lett. 10 (1983) 122.

103. J. H. Yee, V. J. Abreu, and A. Dalgarno, Geo. Res. Lett. 11 (1984) 1192.

104. S. B. Mende, P. M. Banks, and D. A. Klingelsmith III, Geo. Res. Lett. 11 (1984) 527.

105. T. G. Slanger, Geo. Res. Lett. 13 (1986) 431.

106. J. H. Yee and A. Delgarno, AIAA-83-2660 (1983) 191.

107. B. J. Dunbar, Ceramic Bulletin, 60 (1981) 1180.

108. A. Ralston, Mathematics of Computation 16 (1962) 431.

109. N. Sathyamurthy and L. M. Raff, J. Chem Phys. 72 (1980) 3163.

110. P. N. Keating, Phys. Rev. 145 (1966) 637.

111. S. A. Adelman and J. D. Doll, J. Chem. Phys. 64 (1976) 2375.

112. B. J. Garrison and S. A. Adelman, Surf. Sci. 66 (1977) 253.

113. S. A. Adelman and J. D. Doll, J. Chem. Phys. 61 (1974) 4242.

114. J. C. Tully, J. Chem. Phys. 73 (1980) 1975.

115. G. Binnig, H. Rohrer, Ch. Gerber, and E. Weibel, Phys. Rev. Lett. 50 (1983) 120.

116. P. M. Agrawal, D. H. Thompson, and L. M. Raff, J. Chem. Phys. to be published.

117. A. S. Bhandia and J. A. Schwartz, Surf. Sci. 108 (1981) 587.

118. H. Ibach, Surf. Sci. 53 (1975) 444.

119. CRC Handbook of Chemistry and Physics, edited by R. C. Weast (CRC press Inc., Boca Raton, Florida, 1980), 61st Edition.

120. G. Herzberg, Molecular Spectra and Molecular Structure, I. Spectra of Diatomic Molecules. (Van Nostrand Reinhold Co., New York, 1950)

121. L. M. Raff and D. L. Thompson, The Classical Trajectory Approach to Reactive Scattering, in Theory of Chemical Reaction Dynamics, edited by M. Baer (Chemical Rubber, Boca Raton, Florida, 1985), Vol. III, p. 1.

122. L. M. Raff, unpublished work.

123. L. M. Raff, J. Chem. Phys. 89 (1988) 5680.

VITA

Michael W. Jezercak

Candidate for the Degree of

Doctor of Philosophy

Thesis: INVESTIGATION OF METHODS INVOLVED IN THE DYNAMICS OF GAS-SURFACE ENERGY TRANSFER PROCESSES.

Major Field: Chemistry

Biographical:

Personal Data: Born in Oklahoma City, Oklahoma on July 21, 1960, the son of William R. and Irma Jezercak.

Education: Obtained a Bachelor of Science degree from Central State University in the spring of 1983; completed the requirements for a Doctor of Philosophy degree at Oklahoma State University in December, 1989.

Professional experience: Teaching assistant at Central State University in 1984; Graduate assistant at Oklahoma State University department of chemistry from 1984 to 1989, Associate Professor of Chemistry at Central State University, 1989.